SIMULATION OF AN AIR COOLED SINGLE EFFECT SOLAR ABSORPTION COOLING SYSTEM WITH EVACUATED TUBE COLLECTORS

By

Mohsen Jahandardoost

Bachelor of Science in Mechanical Engineering
University of Guilan
2006

A thesis submitted in partial fulfillment
of the requirement for the

Master of Science in Engineering – Mechanical Engineering

Department of Mechanical Engineering
Howard R. Hughes College of Engineering
The Graduate College

University of Nevada, Las Vegas
December 2014

UNLV | GRADUATE COLLEGE

We recommend the thesis prepared under our supervision by

Mohsen Jahandardoost

entitled

Simulation of an Air Cooled Single Effect Solar Absorption Cooling System with Evacuated Tube Collector

is approved in partial fulfillment of the requirements for the degree of

Master of Science in Engineering - Mechanical Engineering
Department of Mechanical Engineering

Robert F. Boehm, Ph.D., Committee Chair

Yitung Chen, Ph.D., Committee Member

Woosoon Yim, Ph.D., Committee Member

Helen Neill, Ph.D., Graduate College Representative

Kathryn Hausbeck Korgan, Ph.D., Interim Dean of the Graduate College

December 2014

ABSTRACT

Simulation of an Air Cooled Single-Effect Solar Absorption Cooling System with Evacuated Tube Collectors

By

Mohsen Jahandardoost

Dr. Robert F. Boehm
Distinguished Professor of Mechanical Engineering
Director, Energy Research Center
University of Nevada, Las Vegas

Consistently increasing CO2 emission and ozone depletion from synthetic refrigerants are serious environmental issues challenging the scientific community. Absorption cooling systems give scope of utilizing low grade energy source for generating cooling effect. Solar energy is one of these low grade energy sources and with considering the fact that cooling demand increases with the intensity of solar radiation, solar refrigeration has been considered as a logical solution.

This thesis consists of two different simulation stages, in the first stage, a single effect lithium bromide absorption cooling system with constant cooling capacity is modeled and the effect of ambient and generator temperatures on concentration and strong solution flow rate is investigated. Then the energy required by the generator and the resulting coefficient of performance (COP) are analyzed by varying all parameters: for instance, strong and weak solution concentration, generator temperature, and ambient temperature. This simulation shows that the generator temperature needs to be increased for higher ambient temperatures and there is one optimum generator temperature that

gives the highest COP. The overall COP after using the control system was between 0.75 and 0.85.

In next stage of the analysis, the sun position and hot water production for cooling season (May through September) in Las Vegas are simulated using TMY3 data and considered using evacuated tube solar collectors. To size the collector area, the hottest day (4^{th} of June at 3 PM) is selected to fulfill the maximum cooling demand and according to amount of solar radiation, ambient temperature, and energy required by generator, the number of collectors is defined. Generally, the solar system is found to be effective and covered 35% of heating demand to run the cooling system continuously through the cooling season.

ACKNOWLEDGMENTS

I would like to express my appreciation to my advisor Dr. Robert Boehm for the continuous support of my master study and my solar and renewable certificate (SRE), for his patience, motivation, and immense knowledge. I also need to mention my sincere gratitude to Dr. Boehm for his guidance in all the time of research and editing of this thesis. I could not have imagined having a better advisor and mentor. He is my role model too.

Besides my advisor, I would like to thank my thesis committee members: Dr. Helen Neill, Dr. Woosoon Yim, and Dr. Yitung Chen. I am appreciative of their time, encouragement, and insightful comments.

I am grateful to Mr. Shaharyar Ahmad for editing the third chapter. And last but not the least, I would like to thank my family, in particular, Mohammad Reza and Azita for their help and support.

DEDICATION

To memory of my Dad,

Who has directed my heart,

you have been such an inspiration to me,

you are always close in my heart,

I never forget you.

To my Mom for loving me unconditionally.

To all my brothers and sisters for

all of the wonderful memories of growing up,

their continued support and encouragement.

TABLE OF CONTENTS

LIST OF TABLES

LIST OF FIGURES

LIST OF SYMBOLS

A_c	collector area [m^2]
B	variable for the equation of time
COP	Coefficient of Performance
C_x	specific heat capacity [kcal/kg °C]
E	equation of time [minutes]
F_R	collector heat removal factor
G_{sc}	solar constant [1367 W/m^2]
h	Enthalpy [$kcal/kg_{solution}$]
H	hour angle [degree]
I	average hourly available irradiation on a plane [W/m^2]
I_b	direct normal irradiance (DNI) [W/m^2]
I_d	diffuse horizontal irradiance (DHI) [W/m^2]
K_T	hourly clearance index
$K_{\tau\alpha}$	incidence angle modifier (IAM)
L	latitude [degrees]
Li – Br	Lithium – bromide solution
L_{loc}	longitude [degrees west of GMT]
L_{st}	standard meridian [degrees]
m	mass [kg]
$\dot{m}$	mass flow rate [kg/s]
n	day number of the year (1 – 365)
Q	heat gain [W, kW or kWh]
r	flow rate correction factor
R_b	geometric factor
S	solar irradiance absorbed at a plane [W/m^2]

t	temperature [degrees Celsius]
TMY	typical meteorological year data
U_L	collector overall heat loss coefficient [W/m^2 °C]
X_1	strong of refrigerant solution concentration [$kg_{Li\text{-}Br}/kg_{solution}$]
X_4	weak of refrigerant solution concentration [$kg_{Li\text{-}Br}/kg_{solution}$]
β	solar altitude angle [degree]
δ	declination [degrees]
ε_L	the heat exchanger effectiveness
η	efficiency of a solar collector
θ	angle of incidence [degree]
θ_z	zenith angle (angle of incidence of beam on a horizontal surface) [degrees]
ρ_g	ground reflectivity
ϕ	azimuth angle [degrees]
Σ	collector tilt angle from the horizontal [degrees]

CHAPTER 1 - LITERATURE REVIEW

Solar refrigeration received intense interest during 1970s when the world suffered from the oil crisis. Solar absorption cooling system is attractive application because of the simultaneous peak in cooling loads with the availability of solar power. There were several projects for the development of solar cooling system and different systems installed and tested around the world.

A 7 kW Li-Br water solar absorption system was installed in a small single story office building in Tokyo and was tested during summer 1974 by Nakahara, Miyakawa, & Yamamoto (1977). The flat plate collectors were used with total area of 32.2 m^2 with design outlet temperature of 75ºC and were connected to an auxiliary gas fired heater. The temperature ranges for different parts of absorption system were 65 – 75ºC, 18 – 25ºC, and 7.5 – 12.5ºC for the generator, the condenser/absorber, and the evaporator, respectively. The collectors showed an efficiency of 0.25 and average outlet temperature of 75ºC with tilt angle of 10º during summer. The experimental data showed with raising the generator inlet temperature from 70ºC to 95ºC, the COP is decreased while the cooling capacity is increased. The overall COP of system was 0.55, and it was concluded that the COP and the capacity are highly dependent to condenser and evaporator temperatures.

Yeung, Yuen, Dunn, & Cornish (1992) designed and constructed a solar powered absorption air conditioning system on the campus of the University of Hong Kong. The system used 20 flat plate solar collectors that were tilted 22.3º and a Li-Br water absorption system with nominal capacity of 4.7 kW. The system was tested during

summer 1986 and the performance of absorption system was found to be reasonable for the cooling season. The collector efficiency during the test period was 37.5%, and the solar air conditioner showed an overall system performance of 7.8 – 8.1% and an average solar fraction of 55%. They concluded the system COP was between 0.57 to 0.6 and cooling capacity ranged from 1.1 to 3.3 kW depending on the thermal power available to the generator.

The effect of using a partitioned hot water storage tank in solar absorption system was investigated by Li & Sumathy (2001). The system was installed in the University of Hong Kong and contained 38 m^2 high performance flat plate collectors and 4.7 kW nominal cooling capacity Li-Br water absorption system. It was tested between June and October 1999. With the tilt angle of 22.3º, the COP of the system was found to be 0.07 which according to authors' claim was 15% higher than the same system with single stage hot water storage tank.

Florides, Kalogirou, Tassou, & Wrobel (2002) modeled and simulated a single stage Li-Br water solar absorption system in Nicosia, Cyprus with the TRNSYS program. They determined the optimum system collector type and size which was a 15 m^2 parabolic collector with a tilt angle of 30° for an 11 kW cooling capacity system.

A single effect solar absorption system with Li-Br water solution as working fluid was modeled and simulated by Atmaca & Yigit (2003) for Antalya, Turkey weather conditions. They examined various absorption cycle and solar energy parameters and found that the increment of the minimum allowable hot water inlet temperature decreases the absorber and heat exchanger surface area and increases the system COP. They also

concluded the system required a high performance collector and an evacuated tube collector was the best option for the effective performance of the absorption system.

Syed et al. (2005) reported on experimental results derived through field testing of a solar absorption cooling system at Carlos III University of Madrid during the summer of 2003. Twenty flat-plate collector modules with total area of 49.9 m^2 and tilt angle of 40º were used to energize the system. A single-effect Li-Br/H_2O absorption chiller of 35 kW nominal cooling capacity, while the generator temperature is 80º, was used. The average COP was demonstrated to be 0.45 with the generator and the absorber temperature range of 57 to 67º and 32 to 36º, respectively. The system also provided 6.4 kW cooling effect at 81ºC hot water inlet temperature to the generator which was 18.3% of nominal capacity.

Assilzadeh, Kalogirou, Ali, & Sopian (2005) simulated a single effect Li-Br water solar absorption cooling system in Malaysia. The TRNSYS program with considering the TMY3 data were used to model and simulate the solar absorption cooling system. They targeted solar heat gain to find the evacuated tube collector slope and the simulation showed that a 20º tilt angle provides the highest heat gain for a 15 m^2 collector area. Their study also suggested a 0.8 m^3 hot water storage tank is necessary to achieve continuous full capacity (3.5 kW) system operation.

Pongtornkulpanich, Thepa, Amornkitbamrung, & Butcher (2008) designed and installed a 35 kW single effect Li-Br/H_2O solar absorption system at the School of Renewable Energy Technology in Phitsanulok, Thailand. The system was installed in 2005, the data were collected over the year 2006, and the system was operated continuously for more than 5 hr when the cooling was required. They showed that a 72

m^2 evacuated tube solar collector provided an average solar fraction of 81%. They also concluded the initial installation costs of system were higher but the operation costs were lower. Balghouthi, Chahbani, & Guizani (2008) analyzed a single effect solar absorption system using TRNSYS and EES software to optimize the collector properties and absorption size for a 150 m^2 building in Tunis, Tunisia. The 30 m^2 flat plate collector with a 35º slope and an 0.8 m^3 hot water storage tank were found to be the optimum solar system component to run 11 kW Li-Br water absorption cooling system.

Rosiek & Batlles (2009) analyzed the 70 kW single stage solar absorption system with 160 m^2 flat plate collector in the campus of University of Almeria in Spain. The collectors were tilted at an angle of 30° to the horizontal line and the generator inlet temperature range was 70 - 95°C with cooling water inlet temperature of 24 to 31°C. The system was tested during the year of 2006 and the average value of COP and cooling capacity were found to be 0.6 and 40 kW, respectively.

A numerical model of the solar absorption system was conducted to predict the performance of control parameters by Ortiz, Barsun, He, Vorobieff, & Mammoli (2010). They refurbished old equipment at the University of New Mexico, Albuquerque's mechanical engineering building in 2006 and used a hybrid solar collector consisting of flat plate and evacuated tube collectors with a tilt angle of 25°. The absorption system was a 70 kW Yazaki single effect Li-Br water chiller with hot water supply temperatures in the range of 70 to 95°. A TRNSYS module was used to model the building, solar loop, and absorption cycle. They illustrated both the COP and cooling capacity were decreased by increasing the outflow temperature of the solar array from 85 to 95°. Mammoli,

Vorobieff, Barsun, Burnett, & Fisher (2010) validated the Ortiz et al. (2010) work with experimental results and found the system could provide 18% of total cooling demand.

Agyenim, Knight, & Rhodes (2010) developed a domestic scale solar absorption system with a 16 m^2 evacuated tube collector and a 4.5 kW single stage Li-Br water absorption system, and ran the system during the summer of 2007 at Cardiff University, UK. The average COP of system and the cooling capacity were 0.58 and 4.07 kW, respectively. In another study, Praene, Marc, Lucas, & Miranville (2011) installed a 30 kW absorption system at the Institute Universitaire Technologique of Sait Pierre, French. The system employed a 90 m^2 flat plate collector and a cooling tower. The maximum cooling capacity was found to be 17 kW during the summer of 2007.

All of the previous studies extensively concentrate on the absorption system performance using a wet cooling tower (that keeps the absorber and the condenser temperatures in the range of 25 to 30°C) and a flat plate collector. Most of them monitored the performance of the system according to the solar radiation, and they didn't provide a strategy for sizing the collector area.

In the present study, an attempt is made to investigate the effect of various parameters on absorption system performance. Various control systems are examined to find the best COP of the system while keeping the concentration in the safe zone to prevent crystallization. Because the system is air cooled, the absorber and condenser temperatures cover a wider range of temperatures, and it is found that the inlet hot water temperature to the generator exceeds the 95°C. A single effect Li-Br water absorption system is modeled to find the best inlet temperature to the generator for a maximum

COP. Then a solar loop is simulated using evacuated tube collectors and Typical Meteorological Year data version 3 for Las Vegas.

CHAPTER 2 – FUNDAMENTALS

2.1 Background

Conventional cold producing machines are based on the vapor compression principle. They are electrically driven and cooling system operation can cause high electrical demand during the summer. This peak load is especially high in tropical climate regions. Their energy usage for both commercial and residential buildings is estimated to be 45% of the whole building energy consumption (Choudhury, Chatterjee, & Sarkar, 2010). Electricity generation from most power plants is dependent on fossil fuels which cause substantial emissions of greenhouse gases to environment.

They also use non natural working fluids, namely, chlorofluorocarbon (CFC), hydrochlorofluoro carbon (HCFC), or hydrofluorocarbon (HFC) as refrigerants which have both high global warming and ozone layer depletion effects. Using these gases contradicts the Kyoto protocol (1998) on global warming and the Montreal Protocol on Substances that Deplete the Ozone Layer (1997).

An alternative solution for these problems is asolar powered cooling system as a green cold production technology. Solar radiation is available in most areas, free for use, and an excellent supply of thermal energy from renewable energy resource and embodied energy related to solar radiation is almost negligible. The most common solar air conditioning alternative is a solar powered absorption system. The absorption system is similar to the conventional vapor compression air conditioning system with this difference that the mechanical compressor is replaced with thermal compressor (the generator and absorber). The mechanical compressor creates the pressure differences

necessary to circulate the refrigerant but in the absorption system, a secondary fluid or absorbent is used to circulate the refrigerant.

In the absorption system, the refrigeration effect is produced by the use of heat instead of electricity, and this heat can be from low grade source like the sun. The main advantage of the solar absorption cooling technology is that the coefficient of performance is higher than other thermally operated cycles, along with low noise and vibration production.

The desirable refrigerant-absorbent combination should be highly soluble in the absorber but should have low solubility in the generator. The combination must not have non-reversible chemical reactions at the operating temperature. The substances should have a large difference in their normal boiling points, as high as 200°C, so that the absorbent exerts negligible vapor pressure at the generator temperature. The viscosity should be low to minimize pump work. There are different kinds of mixtures for absorption system like ammonia (NH_3)/water, lithium-bromide/water, and lithium-chloride/water. In a water-lithium bromide vapor absorption refrigeration system, water is used as the refrigerant while lithium bromide (Li-Br) is used as the absorbent.

There are advantages and disadvantages of the Li-Br solution. The advantages of the system include high safety, affinity, latent heat, and stability. The Li-Br solution is not volatile and the working pair is odorless and neither toxic nor flammable. High affinity allows less absorbent to be circulated for the same refrigeration effect, reducing sensible heat losses, and allows a smaller liquid heat exchanger. Also the refrigerant (water) latent heat is high, so the circulation rate of the refrigerant and absorbent is small. The cons of solution include the difficulty of operating at temperatures lower than 0°C

because the refrigerant has a high freezing point. Besides, Li-Br crystallizes at moderate concentration. The solution is corrosive to some metals and has high cost. The system operates below atmospheric pressure, resulting in system air infiltration, which requires periodical purging.

2.2 Objectives

The first objective of this project is the development of a solar absorption cooling configuration as a result of system simulations. There are extensive studies on solar absorption cooling systems that use a cooling tower and consequently, the condenser temperature is limited in the range of 25°C to 30°C so the required temperature in generator is dropped to 90°C. The cooling tower increases the cost of the system, results in water usage, and has a large system volume. In this simulation, a programming model is developed for Li-Br/water absorption system with an air-to-air condenser and absorber to be used in remote areas with limited access to electricity.

The next objective is to investigate the effect of different parameters on the solar absorption cooling system performance. The cooling load and chilled water temperature are assumed to be constant. In this approach the system is assumed to work all the time when the ambient temperature is higher than 20°C. Also the condenser and absorber temperatures are assumed to equal the ambient temperature. The solution concentration is highly sensitive to temperature in the condenser and generator. Another important parameter is solar insolation which provides heat in generator. Solution flow rate and water flow rate in the collector loop are additional temperature-dependent components.

One final objective is to show the effect of controlling these parameters on system performance. Different combinations are presented and the goal is set to achieve the highest COP while staying in a safe concentration zone. With using an appropriate control system, the COP between 0.75 and 0.85 can be achieved for any ambient temperature.

2.3 Absorption Cooling System

An absorption refrigeration cycle uses the principles of heat transfer and change of phase of the refrigerant to produce the refrigeration effect. The system provides a cooling effect by absorbing heat from one fluid (chilled water) and transferring it to another fluid (cooling water or ambient air). It also uses a device (thermal compressor) to increase the pressure of the refrigerant and an expansion device to maintain the internal pressure difference.

There are two fundamental differences between the absorption cycle and the vapor compression refrigeration (VCR) cycle. First, the mechanical compressor in VCR is replaced by an absorber, pump, and generator (thermal compressor). Second, the absorption refrigeration cycle uses a secondary fluid (absorbent) to carry the refrigerant from the low-pressure side (evaporator) to the high-pressure side (condenser). Figure 2.1 shows a schematic of solar absorption cooling system.

2.3.1 Absorption Component

The single effect[1] absorption cooling system contains of four basic components which are the generator and condenser on the high-pressure side, and the evaporator and

[1] The number of the effect in the cycle signifies the number of times the driving heat is used in the cycle so a single effect means that there is one generator in the system.

absorber on the low-pressure side. The pressure on the high-pressure side of the system is approximately ten times greater than that on the low-pressure side. At atmospheric pressure (14.7 psia or 101.3 kPa), water boils and evaporates at 212°F or 100°C and when the pressure is decreased, water boils at a lower temperature. The pressure in evaporative side is very low, near 1 kPa, so the water boils in lower temperature, 7.5°C, and therefore refrigerant can absorb heat from chilled water which works at atmospheric pressure and produces cooling effect (ASHRAE, 1997).

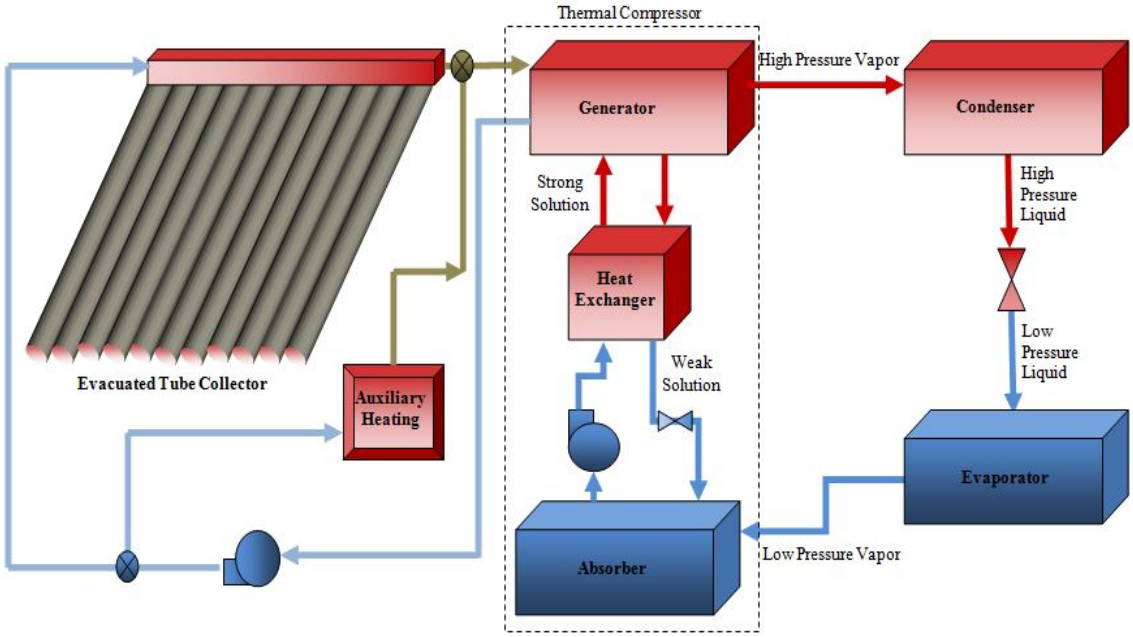

Figure 2.1 Schematic diagram of solar absorption cooling system

The generator is on the high pressure side of the cycle and designed to deliver the refrigerant to the rest of the system. It uses heat to separate the refrigerant from the solution. Because the boiling point of Li-Br is higher than water, it is easy to vaporize the water at low pressure and remove it from the solution. A high temperature energy source (heat generated by the sun) flows into the strong refrigerant solution, and the solution

absorbs this heat which causes the water to vaporize. This results in a high Li-Br concentrated solution. The hot and weak refrigerant solution goes through the heat exchanger and enters the absorber.

The pressure in the condenser is less than in the generator because the temperature on the generator is higher than the condenser. The high pressure vapor refrigerant migrates to the cooler condenser and becomes liquid by exchanging heat with the ambient temperature. Then the high pressure liquid refrigerant passes through the expansion valve to reduce its pressure. This causes some part of the refrigerant to boil again and reduces the temperature of liquid-vapor mixture entering the evaporator. Inside the evaporator, the low temperature liquid-vapor refrigerant gets in contact with the warm return-water from the chilled water system and becomes fully vaporized.

The warm and rich Li-Br solution has a strong affinity to absorb this low-pressure vapor refrigerant on the absorber side. During this process, the refrigerant condenses from vapor to liquid which releases heat. This heat disperses to the ambient temperature in the absorber. The lower pressure in the absorber, in addition to the solution's attraction to water, causes continuous flow of refrigerant from the evaporator to the absorber. The strong refrigerant solution pumps to the generator and the cycle repeats again. The cool strong solution passes through the heat exchanger to be in contact with the hot weak solution. This heat transfer preheats the strong solution and reduces the heat energy required to boil the refrigerant within the generator and also cools the weak solution.

Lithium bromide is a salt and has a naturally occurring crystalline structure. When the temperature of the solution with constant mass fraction of Li-Br drops below saturation temperature, or when the concentration of Li-Br of the solution with constant

temperature is higher than the saturated concentration in same temperature, the part of Li-Br exceeding the saturated condition forms solid crystals. A wet solid or slush can occur in the piping by crystallization, and over time it could form a solid and block the flow. Crystallization can be avoided by adding heat in that area or diluting the solution with water from the evaporator (Herold, Radermacher, & Klein, 1996).

Properties of the Li-Br water solution can be illustrated by an equilibrium chart based on a Duhring (ASHRAE, 1997) plot (solution temperature versus reference temperature). Figure 2.2 illustrates this chart where the saturated vapor pressure of water is the vertical axis in a log-scale millimeter of mercury absolute (mmHg abs) versus the corresponding solution temperature (°C). This line also represents the saturated vapor temperature (°C) of refrigerant. Mass fraction or concentration lines are inclined lines and are not parallel to each other, and the crystallization line (saturation line) is at the bottom of concentration lines.

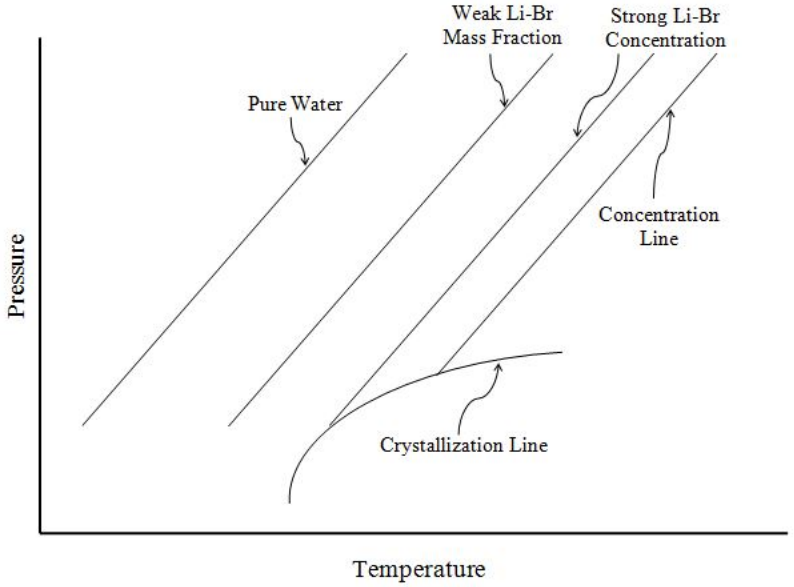

Figure 2.2 Single effect water Li-Br absorption cycle Duhring plot

2.3.2 Thermodynamic of Cycle

To model an absorption cycle, four types of thermodynamic equations need to be considered, namely, mass balances, energy balances, relations between heat and mass transfer, and equations for thermophysical properties of the refrigerant. A flow diagram of single effect Li-Br water absorption cycle is shown in Figure 2.3. The heat is used to boil the water and separate it from the Li-Br solution and increase the mass fraction of Li-Br in the solution (X_4). The high pressure water vapor passes to the condenser, state 7, where heat is removed and the refrigerant cools to a liquid, state 8. The expansion valve changes the refrigerant pressure to a lower level, state 9, which causes some part of the refrigerant to boil again and a mixture of liquid-vapor refrigerant enters the evaporator.

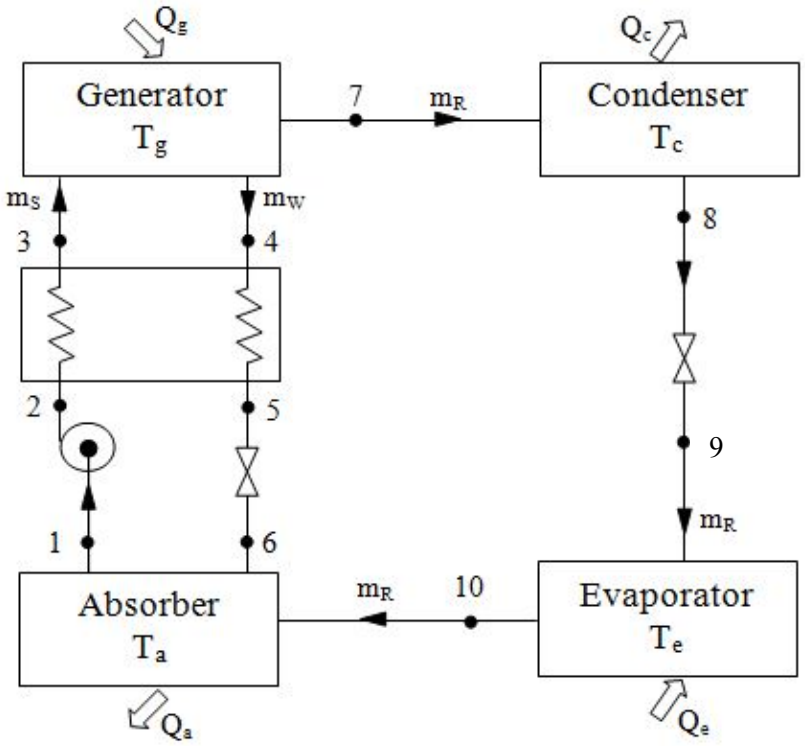

Figure 2.3 Flow diagram for a single stage Li-Br water absorption system

At the evaporator, the low pressure refrigerant is introduced to the atmospheric pressure water in the chiller loop and heat is transferred from the chilled water to the refrigerant at an amount equal to the latent heat of vaporization. The low pressure water vapor goes to the absorber because of the lower pressure in the absorber and also high affinity of Li-Br to water, state 10. Meanwhile, the hot weak solution passes through a heat exchanger to preheat the strong solution entering the generator, state 3, and also a cooler solution enters the absorber, state 5, reducing the amount of heat transfer in the absorber. In the absorber, Li-Br absorbs the water from the evaporator to form a strong of refrigerant solution. Since the absorption process is exothermic, the latent heat of the phase change of the refrigerant is released to the ambient in order to keep the absorber at the evaporator low pressure. The circulating pump brings the strong solution from the low pressure absorber to the high-pressure generator, state 2, and the process is repeated by absorbing heat in the generator. The thermodynamic cycle of a single stage Li-Br water absorption cooling system is given on the equilibrium chart for different states at various concentrations, temperatures, and pressures as shown in Figure 2.4.

The concentration of solution can be defined as the ratio of the mass of Li-Br to the total mass of the solution which is given as:

$$X = \frac{m_{Li\text{-}Br}}{m_{Li\text{-}Br} + m_{Water}} \tag{2.3.1}$$

ASHRAE (1997) suggests the following set of equations to calculate the concentration in the Li-Br water solution:

$$t = \sum_0^3 B_n X^n + t' \sum_0^3 A_n X^n \tag{2.3.2}$$

$$t' = \frac{\left(t - \sum_0^3 B_n X^n\right)}{\sum_0^3 A_n X^n} \tag{2.3.3}$$

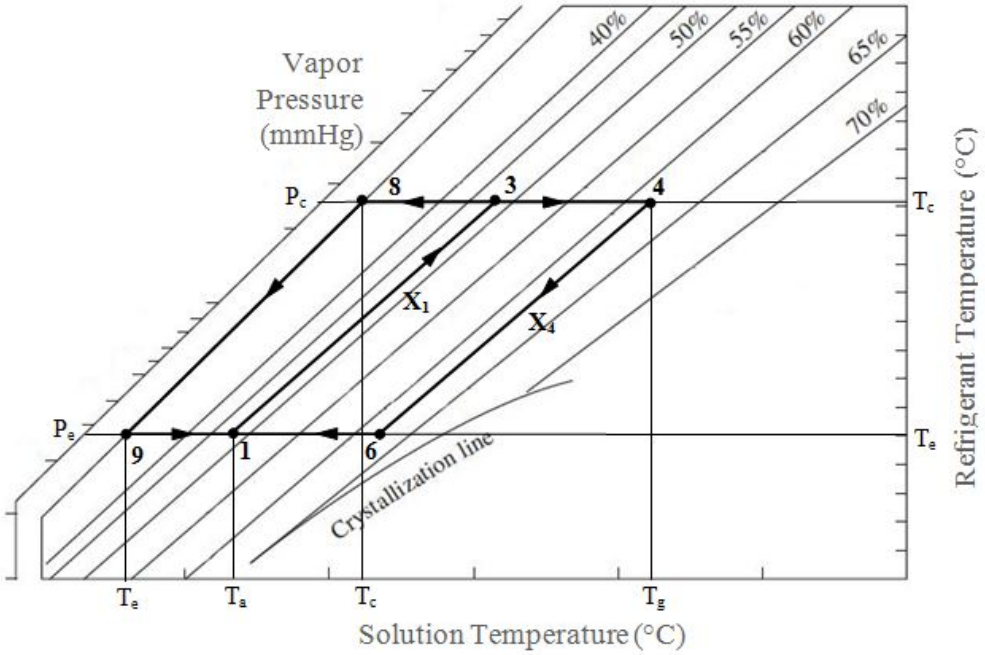

Figure 2.4 Equilibrium chart for Li-Br water solution

Where t is solution temperature and t' is the refrigerant temperature, and both of them are in °C and X is the concentration of the solution in percentage. The A_n and B_n are the equation constants and are given in Table 2.1.

Table 2.1 Constants for use in Equations 2.3.2 and 2.3.3

$A_0 =$	2.00755	$B_0 =$	124.937
$A_1 =$	0.16976	$B_1 =$	–7.71649
$A_2 =$	-3.1334×10^{-3}	$B_2 =$	0.152286
$A_3 =$	1.9767×10^{-5}	$B_3 =$	-7.9509×10^{-4}

The enthalpy of the solution is given as (ASHRAE, 1997):

$$h = \sum_0^4 A_n X^n + t \sum_0^4 B_n X^n + t^2 \sum_0^4 C_n X^n \qquad (2.3.4)$$

Here h is the solution enthalpy in kJ/kg, t is the solution temperature in °C and X is the solution concentration in percentage. The A_n , B_n , and C_n are equation constants and are given in Table 2.2.

Table 2.2 Constants for Equation 2.3.4

$A_0 =$	–2024.33	$B_0 =$	18.2829	$C_0 =$	-3.7008×10^{-2}
$A_1 =$	163.309	$B_1 =$	–1.169175	$C_1 =$	2.8878×10^{-3}
$A_2 =$	–4.88161	$B_2 =$	3.24804×10^{-2}	$C_2 =$	-8.1313×10^{-5}
$A_3 =$	6.3029×10^{-2}	$B_3 =$	-4.0342×10^{-4}	$C_3 =$	9.9117×10^{-7}
$A_4 =$	-2.9137×10^{-4}	$B_4 =$	1.8521×10^{-6}	$C_4 =$	-4.4441×10^{-9}

The pressure in the absorption cooling system can be found through the following equations:

$$\text{Log } P = C + \frac{D}{T'} + \frac{E}{T'^2} \tag{2.3.5}$$

$$T' = \frac{-2E}{D + \left[D^2 - 4E(C - \log P)\right]^{0.5}} \tag{2.3.6}$$

Here T' is the refrigerant temperature in degree Kelvin and P is the system pressure in kPa. The C, D, and E are the equation constants and according to the ASHRAE (1997), are given as 7.05, –1596.49, and –104095.5, respectively.

The enthalpy of saturated water at temperature t is found from following equation (Miao, 1978):

$$h_{10} = (572.8 + 0.417\ t_e) \tag{2.3.7}$$

Where h_{10} is in kcal/kg and t_e is the low pressure vapor temperature after the evaporator in °C. The enthalpy of superheated steam at temperature t_g (°C) and pressure equal to the saturation pressure of the steam at temperature t_c by taking the specific heat of water vapor equal to 0.46 kcal/kg is given as:

$$h_7 = 572.8 + 0.46\ t_g - 0.043\ t_c \qquad (2.3.8)$$

The specific heat (kcal/kg solution °C) of Li-Br water solution at concentration X (kg Li-Br/kg solution) is equal to (Miao, 1978):

$$C_x = 1.01 - 1.23\ X + 0.48\ X^2 \qquad (2.3.9)$$

Because a throttling process is isenthalpic, the enthalpy of water entering the evaporator, h_8, is equal to the enthalpy of saturated liquid leaving the condenser, h_9, so the flow rate of refrigerant can be calculated as

$$\dot{m}_r = \frac{Q_e}{h_{10} - h_8} \qquad (2.3.10)$$

Where Q_e is the cooling load in kcal/hr and h_8 is the enthalpy of pure water liquid at the evaporator temperature and can be calculated from a psychometric chart. According to mass balance in the absorber, the flow rate of weak and strong solution can be calculated:

$$\dot{m}_r\ X_{10} + \dot{m}_w\ X_6 = \dot{m}_s\ X_1 = (\dot{m}_r + \dot{m}_w)\ X_1 \qquad (2.3.11)$$

$$X_4 = X_5 = X_6 = X_w \qquad (2.3.12)$$

$$X_1 = X_2 = X_3 = X_s \qquad (2.3.13)$$

$$X_7 = X_8 = X_9 = X_{10} = 0 \qquad (2.3.14)$$

By using equations 2.3.12 to 2.3.14 and substituting the concentrations into equation 2.3.11, the mass flow rate of the weak and strong solutions are given as:

$$\dot{m}_w = \dot{m}_r \left(\frac{X_1}{X_4 - X_1}\right) \qquad (2.3.15)$$

$$\dot{m}_s = \dot{m}_r \left(\frac{X_4}{X_4 - X_1}\right) \qquad (2.3.16)$$

In the liquid-liquid heat exchanger between the absorber and generator, the difference of the specific heat in the weak solution side (state 3) is the minimum so the heat exchanger effectiveness is (London, Kraus, Shah, & Metzger, 1990):

$$\varepsilon_L = \frac{t_g - t_5}{t_g - t_a} \tag{2.3.17}$$

From above equation, the temperature of weak solution leaving the heat exchanger and entering the absorber can be calculated as:

$$t_5 = t_g - \varepsilon_L (t_g - t_a) \tag{2.3.18}$$

And from strong solution side:

$$\varepsilon_L = \frac{(\dot{m}_s\ C_{X1})\cdot(t_3 - t_a)}{(\dot{m}_w\ C_{X4})\cdot(t_g - t_a)} \tag{2.3.19}$$

The strong solution temperature leaving the heat exchanger and entering the generator can be calculated by rearranging equation 2.3.19:

$$t_3 = t_a + \left[\varepsilon_L \left(\frac{X_1}{X_4}\right) \left(\frac{C_{X4}}{C_{X1}}\right) (t_g - t_a)\right] \tag{2.3.20}$$

The heat balance for different components of the absorption system, condenser, absorber and generator, are given as:

$$Q_c = m_r (h_7 - h_8) \tag{2.3.21}$$

$$Q_g = m_r h_7 + m_w h_5 - m_s h_1 \tag{2.3.22}$$

$$Q_a = m_r h_{10} + m_w h_5 - m_s h_1 \tag{2.3.23}$$

Since the pump work is negligible and the process is assumed adiabatic, the enthalpies before and after the pump become equal ($h_1 = h_2$).

The coefficient of performance (COP) is defined as the fraction of the cooling provided by system to the total heat introduced to the system and is given as (Miao, 1978):

$$COP = \frac{\text{refrigeration effect}}{\text{external heat input}} = \frac{Q_e}{Q_g} \tag{2.3.24}$$

Or

$$COP = \frac{(h_{10} - h_8)(X_4 - X_1)}{[X_1 h_5 + (X_4 - X_1) h_7 - X_4 h_1]} \tag{2.3.25}$$

2.3.3 Control Strategy

In order to model a single-effect solar absorption cooling system, it is important to have a control strategy. Two control strategies are investigated in this study, namely: concentration control and water flow rate control in the solar loop. The crystallization happens when the temperature of the solution drops below the crystallization line on the equilibrium chart and causes a decrease on the concentration of the remaining solution. The condenser and absorber temperatures highly impact the concentration, and here their temperatures are assumed to be equal to the ambient temperature so the concentration is varied by changing the ambient temperature.

Using a variable speed pump in the solar loop allows the control of water flow rates to the collectors and consequently the control of the temperature in the generator. It is derived from the information covered in the next section. There it is assumed that the total absorbed solar radiation by collectors is constant over each hour. This means that by changing the water flow rate, the output temperature from the collectors can be changed and it varies the heat input to the generator. Using this variable helps the program to

simulate the solar absorption system to find the best concentration and COP for each given ambient temperature.

2.4 Solar Radiation

Solar energy can be harvested directly in two forms, electricity or heat. The electricity is obtained by photovoltaic material which absorbs the sunlight and transforms it to electricity. Solar thermal is another technology related to solar energy which heat is transferred from sunlight to a working fluid like water by a solar collector. The useful heat gain from solar radiation is dependent to the amount of solar flux which is different during the time of day and through the year and the receiver which can be in any orientation and efficiency. From this point, knowing the characteristics of collector and sun position are important to predict the system performance. In the following section, the required equations to predict the incident solar radiation and the collectors' heat production are investigated.

2.4.1 Sun Position

It is essential to know the position of the sun at any time during the year for any geographical location to design and analyze the solar system. The rotation of earth around the sun happens every 365.25 days in an elliptical orbit. The earth also rotates around its axis and this spin is 360.99°, which produces 24 hours during each day (Masters, 2004). In the northern hemisphere, the inclination of the North Pole reaches its lowest angle away from the sun on the 21st of June which produces the longest day during year and is called the summer solstice. See Figure 2.5. In contrast, the shortest day during year happens on the 21st of December and is called the winter solstice.

There are also two days during a year where the lengths of day and night are equal and these are called the equinox. Figure 2.5 also shows another important factor on earth orbit which is the earth's spin axis. It is tilted 23.45° relative to the ecliptic plane (earth's orbit plane around the sun).

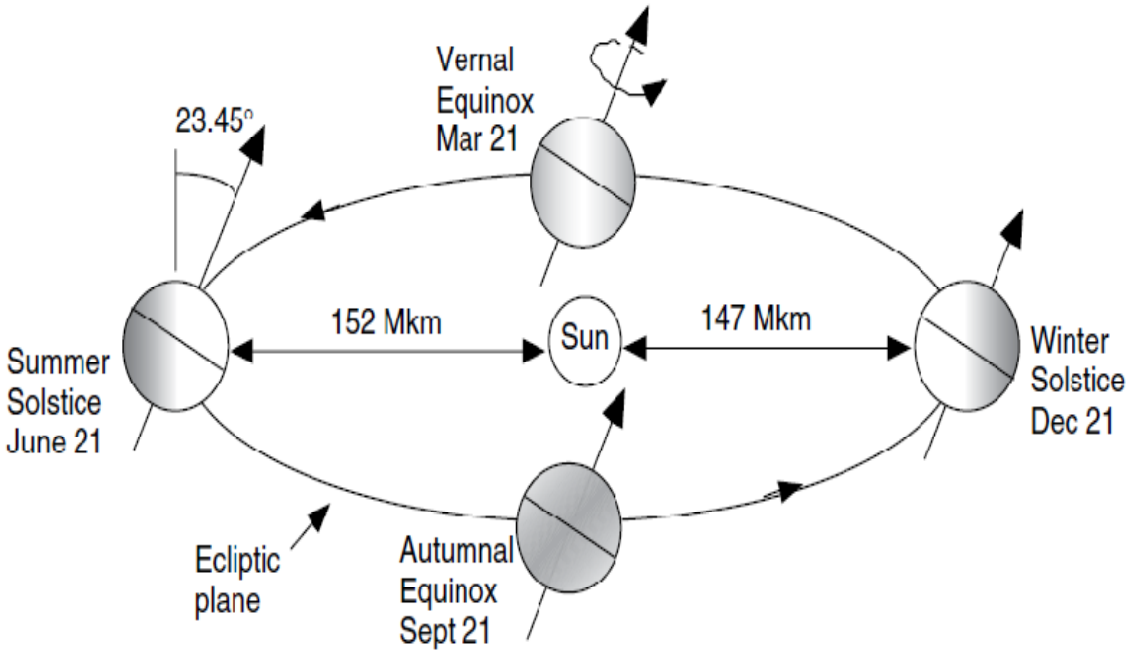

Figure 2.5 Earth position relative to the sun (Masters, 2004)

The site location such as latitude and longitude and climate conditions like ambient temperature, wind speed, and cloud cover are important to determine the sun location and the collector performance. The geometric relations between sun and collector can be presented through different angles and equations. One of these angles is the solar declination, δ, which is defined as the angle between the plane of the equator and a line drawn from the center of the sun to the center of the earth as shown in Figure 2.6. This angle varies between +23.45° to −23.45° from summer to winter and can be found by following equation:

$$\delta = 23.45 \sin\left(\frac{360\,(284 + n)}{365}\right) \tag{2.4.1}$$

Here n is day number and changes from 1 on first of January to 365 on end of December.

The solar declinations for the 21st of each month are listed in Table 2.3.

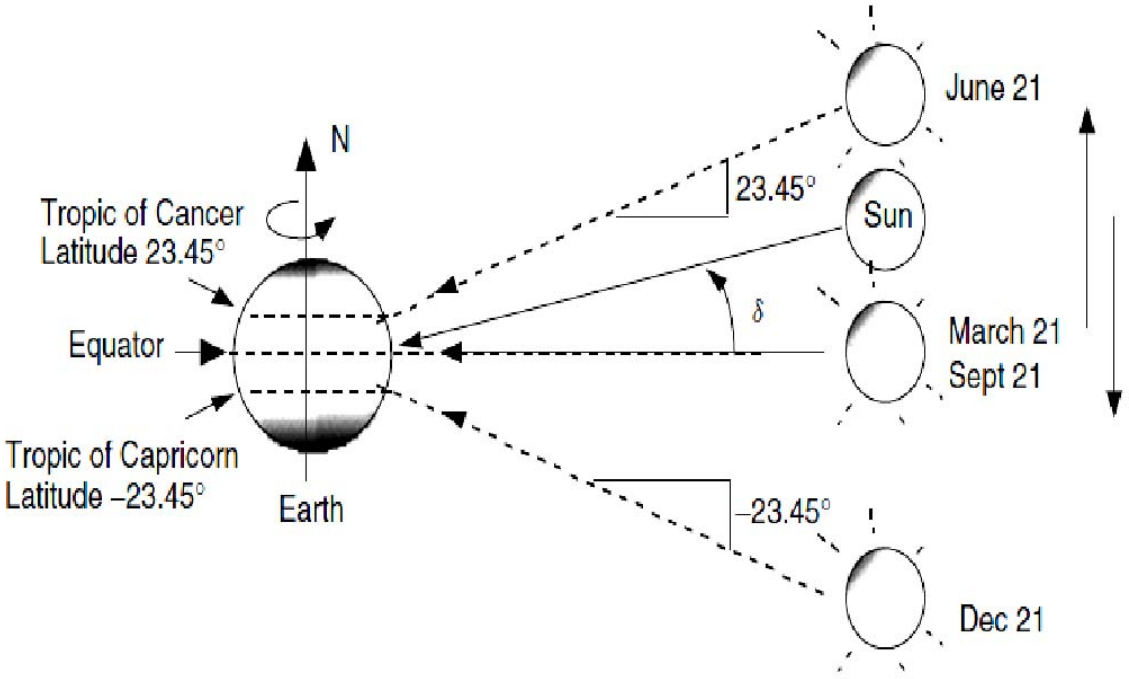

Figure 2.6 Solar declination angle (δ) is shown (Masters, 2004).

Table 2.3 Solar Declination (δ) for the 21st Day of Each Month (°) (Masters, 2004)

Month	Declination	Month	Declination
Jan.	−20.1	Jul.	20.4
Feb.	−11.2	Aug.	11.8
Mar.	0	Sep.	0
Apr.	11.6	Oct.	−11.8
May.	20.1	Nov.	−20.4
Jun.	23.4	Dec.	−23.4

The sun position also needs to be defined by the location of the sun during a day relative to the site orientations. Figure 2.7 shows some of these angles. The solar altitude angle, β, is defined as the angle between the horizontal line and the line to the sun. The smaller magnitudes of this angle mean the sun is closer to horizon which happens during winter. The solar azimuth angle is the angular displacement of the sun from south of the projection of beam radiation on the horizontal plane (Duffie & Beckman, 2006). This angle is positive when the sun is east of south and is negative when it is west of south, as shown in Figure 2.7.

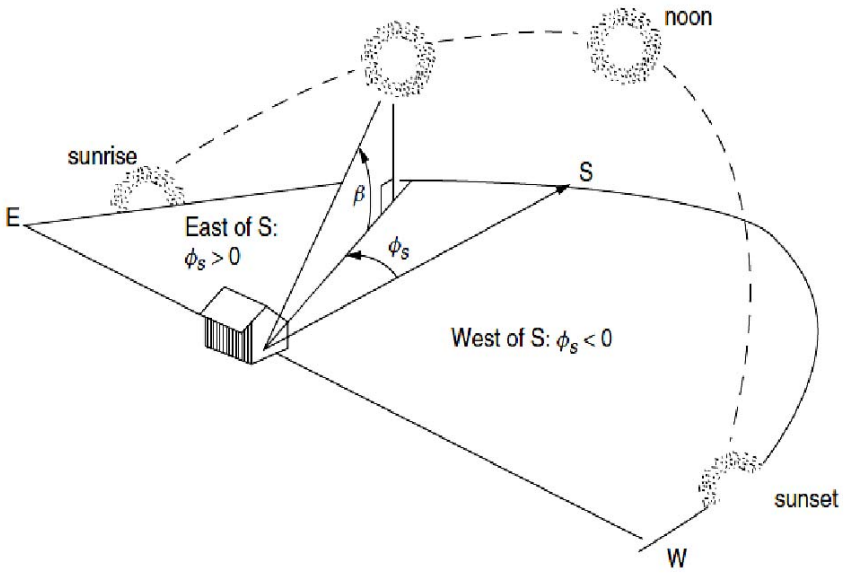

Figure 2.7 Solar altitude (β) and azimuth angles (ϕs) (Masters, 2004)

The following equations describe the relation of solar altitude and azimuth angles with latitude (L) and hour angle (H) (Kuehn and Ramsey, 1998):

$$\sin\beta = \cos L \cos\delta \cos H + \sin L \sin\delta \tag{2.4.2}$$

$$\sin\phi_s = \left(\frac{\cos\delta \sin H}{\cos\beta}\right) \tag{2.4.3}$$

Here L is the local latitude, and H is the hour angle. The hour angle is the number of degrees that the earth must rotate before the sun will be directly over the local meridian and is equal to 15° divided by the solar time (Masters, 2004). The hour angle is positive in the morning and negative in the afternoon. The solar time is based on the apparent angular motion of the sun across the sky. At solar noon, the sun is in the middle of its path from east to west which is usually different from noon local time. The relation between solar time and local time is (Duffie & Beckman, 2006):

$$\text{Solar time} - \text{Local time} = 4\,(L_{st} - L_{loc}) + E \tag{2.4.4}$$

L_{st} is the local time meridian in degrees which is located in the middle of each time zone, L_{loc} is the longitude of the site in degrees, and E is the equation of time. The equation of time in minutes is the result of the elliptical orbit of the earth and is given as:

$$E = 0.02292\,(0.\,75 + 18.68\cos B + 320.77\sin B - 146.15\cos 2B - 408.9\sin 2B \tag{2.4.5}$$

$$B = (n - 1)\,\frac{360}{365} \tag{2.4.6}$$

Here n is the day number, and E varies between –15 min and +17 min

The total solar radiation received by a collector is a combination of direct beam, diffused beam, and reflected beam. Direct radiation or beam passes in a straight line through the atmosphere to the receiver, Figure 2.8. Diffuse radiation is scattered solar radiation in the atmosphere by water molecules and aerosols. The sum of beam and the diffuse radiation on a horizontal surface is called the global horizontal radiation. Reflected radiation may come from the ground or other surfaces in front of the collector. It is related to the ground reflectivity, ρ_g, and the global horizontal radiation. Estimates of

ground reflectance range from about 0.8 (snow) to 0.1 with a typical value of 0.2 for ordinary ground or grass.

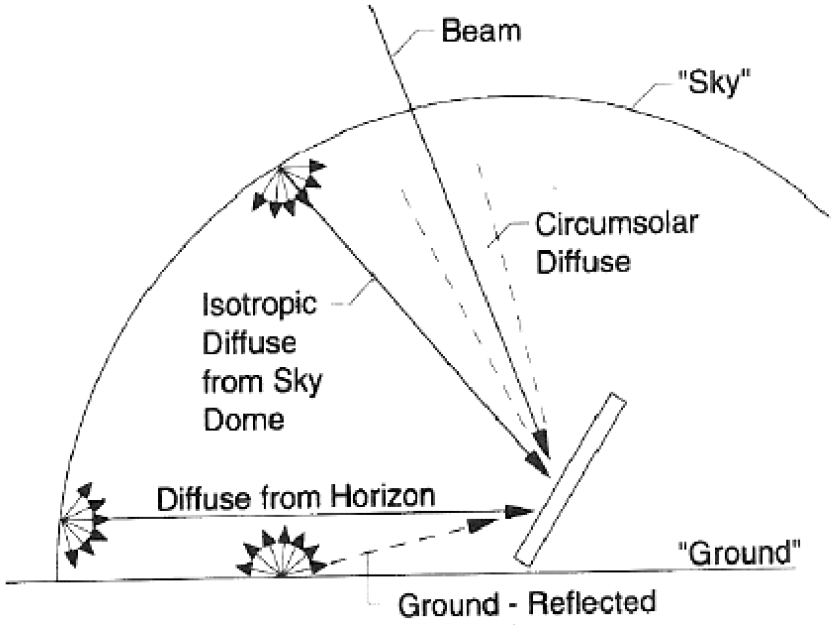

Figure 2.8 Direct, diffused, and reflected solar radiation (W/m^2) (Duffie & Beckman, 2006)

The relations between solar radiation and collectors' tilt angle (Σ), Figure 2.9, can be derived from the following set of equations (Duffie & Beckman, 2006):

$$\frac{I_d}{I_g} = \begin{cases} 1 - 0.09\,k_T & k_T \le 0.22 \\ 0.9511 - 0.16\,k_T + 4.388\,k_T^2 - 16.638\,k_T^3 + 12.336\,k_T^4 & 0.22 < k_T \le 0.8 \\ 0.165 & k_T > 0.8 \end{cases} \quad (2.4.7)$$

$$k_T = \frac{I_g}{I_0} \quad (2.4.8)$$

$$I_0 = G_{sc}\left(1 + 0.33\cos\frac{360\,n}{365}\right)\cos\beta \quad (2.4.9)$$

Where I_d is the diffuse radiation, I_g is total global horizontal radiation, k_T is the hourly clearness index, I_0 is extraterrestrial radiation which is the solar energy received on a

horizontal surface outside of the atmosphere, G_{sc} is the solar constant (1367 W/m^2), and n is the day number.

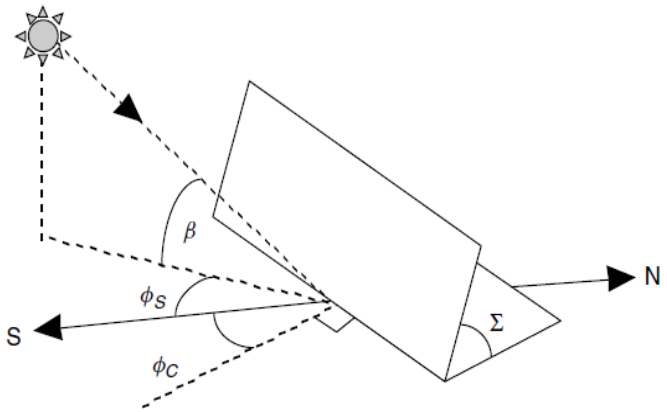

Figure 2.9 Illustration of tilt (Σ), solar altitude (β), solar azimuth (ϕ_s), and surface azimuth (ϕ_c) angles (Masters, 2004)

After finding the ratio of diffused radiation to global radiation, the diffuse radiation can be calculated by multiplying this ratio with the global radiation. The direct beam can be found by subtracting the diffused radiation from global radiation ($I_b = I_g - I_d$). Then the total radiation on a tilted surface, Figure 2.8, is given by (Duffie & Beckman, 2006):

$$I_{bc} = I_b R_b \tag{2.4.10}$$

$$R_b = \frac{\cos\theta}{\sin\beta} = \frac{\cos\theta}{\cos\theta_Z} \tag{2.4.11}$$

$$\cos\theta_Z = \cos L \cos\delta \cos H + \sin L \sin\delta \tag{2.4.12}$$

$$I_{dc} = I_d \left(\frac{1 + \cos\Sigma}{2}\right) \tag{2.4.13}$$

$$I_{rc} = I_g \rho_g \left(\frac{1 - \cos\Sigma}{2}\right) \tag{2.4.14}$$

Here I_{bc} is the beam radiation incident on a tilted collector, R_b is the geometric factor which is the ratio of beam on a tilted surface to a beam on a horizontal surface at any time. In this representation θ is the angle of incidence, β is the altitude angle, θ_z is the zenith angle (the angle between vertical and the line to the sun), I_{dc} is the diffuse radiation on tilted surface, Σ is tilt angle, I_{rc} is reflected radiation on the tilted surface, and ρ_g is the ground reflectivity. The total solar radiation on a tilted surface is the sum of beam, diffused, and reflected radiation from equations 2.4.10, 2.4.13, and 2.4.14 is:

$$I_c = I_{bc} + I_{dc} + I_{rc} \tag{2.4.15}$$

Solar radiation data are available in several forms and two most common sources of them are data manual for flat plate and concentrating collectors (Redbook) and typical meteorological year data (TMY). The Redbook was produced by the National Renewable Energy Laboratory (NREL) and contains the average monthly and yearly solar radiation for the period of 1961 – 1990 for several locations in the US. Minimum and maximum values are also included to show the variability of a station's solar resource. The document also gives climatic conditions such as ambient temperature and wind speed (Marion & Wilcox, 1994). The first set of TMY data was produced by Sandia National Laboratory in 1978, and NREL updated it in 1994. The method behind the creation of the TMY3 data is an empirical approach such that individual "typical" months are selected from different years over a period of 30 years (1976 – 2005). The TMY3 data set is composed of 12 typical meteorological months by considering the five most important elements, namely, global horizontal radiation, direct normal radiation, dry bulb temperature, dew point temperature, and wind speed (Wilcox & Marion, 2008). The

TMY3 data for the cooling season, April – September, in Las Vegas is selected for the solar absorption cooling system simulation in this study.

2.4.2 Evacuated Tube

Flat plate collectors and evacuated tube collectors are the two most well-known solar collectors for heating fluids by sunlight. Evacuated tube collector efficiency is lower but this type can increase water temperature higher than can a flat plate collector, Figure 2.10. They also perform better during cloudy, rainy, and windy weather conditions (Duffie & Beckman, 2006). The evacuated tube collector consists of vacuum sealed glass tube as shown in Figure 2.11. Its configuration is an external glass envelope, an internal absorber plate, and a heat pipe containing a transfer fluid.

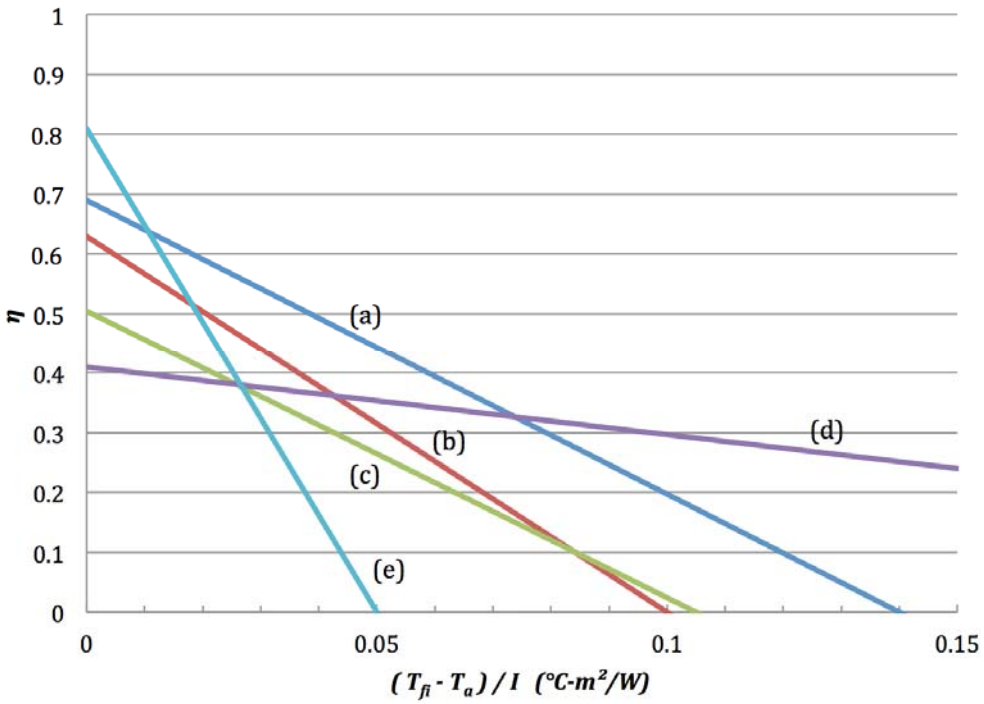

Figure 2.10 Efficiency of different collectors, (a) liquid flat plate, (b) liquid flat plate with black paint absorber, (c) air heater, (d) evacuated tube, and (e) unglazed liquid flat plate (Based on Duffie & Beckman, 2006.)

The glass envelope has two glass tubes within each other which are joined at the end of the collector and create a vacuum layer around the central absorber and heat pipe. The sun's radiation is absorbed by the copper pipe inside the glass envelope and heats the internal fluid to the boiling point. The glass tubes are evacuated which reduces the heat loss from the hot copper tubes. This hot fluid is in contact with water from the solar loop at the manifold in the top of the collector where it heats the water.

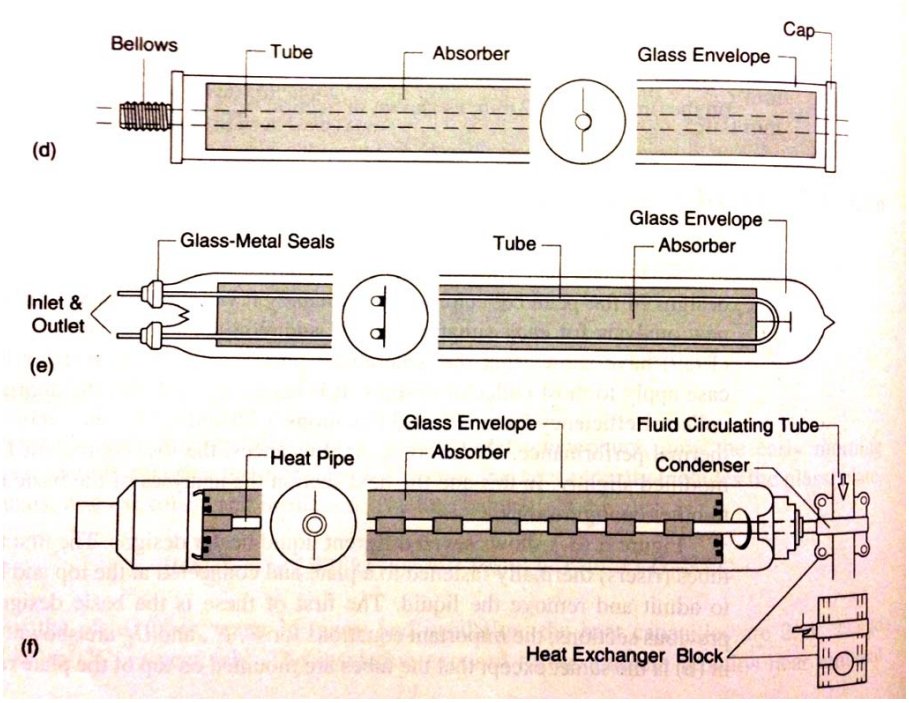

Figure 2.11 Different kinds of evacuated tube collectors are shown (Duffie & Beckman, 2006)

The performance of evacuated tube collectors depends on transmission of sunlight through the glass cover for different incident angles. Because the tubes are optically nonsymmetrical, Figure 2.12, the biaxial incidence angle modifiers need to be used as recommended by McIntire & Reed (1983). An overall incidence angle modifier ($K_{\tau\alpha}$) is

taken as the product of transverse and longitudinal incidence angle modifier (IAM) and is given by:

$$K_{\tau\alpha} = (K_{\tau\alpha})_t \, (K_{\tau\alpha})_l \qquad (2.4.16)$$

The IAM is dependent on the type of glass used for the evacuated tube and this varies from one manufacturer to another. One of the best sources of IAM data is the Solar Rating and Certification Corporation (SRCC) data sheet. They evaluate different collectors from different manufacturers under a variety of parameters and produce transverse incident angle modifiers (IAM_t) for selected angles from 10° to 70°.

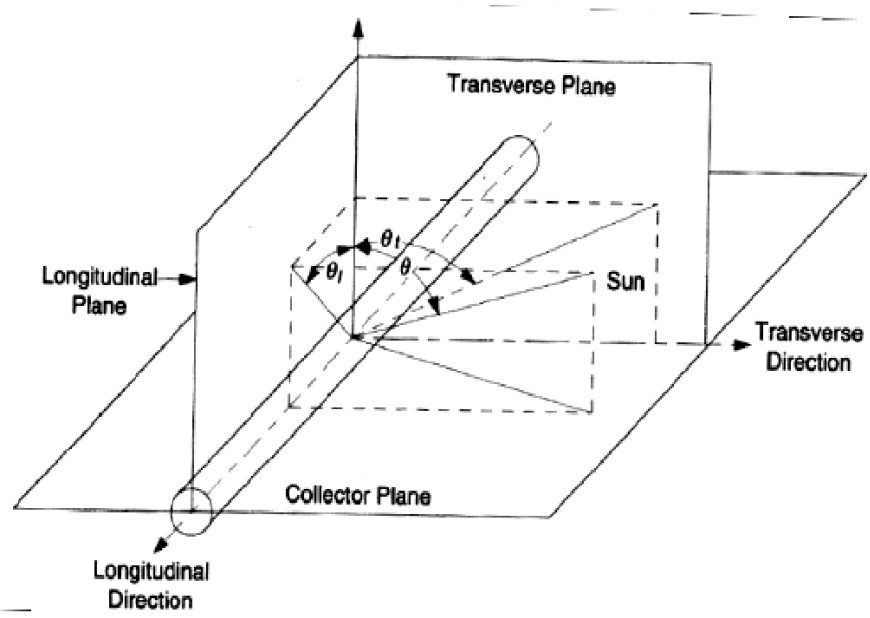

Figure 2.12 The planes of the evacuated tube incident angle modifiers (Duffie & Beckman, 2006)

Sometimes the longitudinal incident angle modifier (IAM_l) and the transmittance of the glass (τ) are not given by the manufacturer or the SRCC, like the evacuated tube collector selected for this simulation (SolarUS SL-30), which in those cases, the IAM_l is

considered to be unity. Figure 2.13 shows the IAM_t from the experimental data from the SRCC and a polynomial curve fitted to those points and the equation representing this polynomial curve is:

$$(K_{\tau\alpha})_t = -4\times10^{-10}\,\theta^6 + 5.87\times10^{-8}\,\theta^5 - 3.74\times10^{-6}\,\theta^4 + 1.13\times10^{-4}\,\theta^3 - 1.42\times10^{-3}\,\theta^2 + 8.18\times10^{-3}\,\theta + 1 \quad (2.4.17)$$

For a solar incident angle smaller than 10 degrees, the IAM is considered to be unity, and for θ higher than 70°, it is assumed zero.

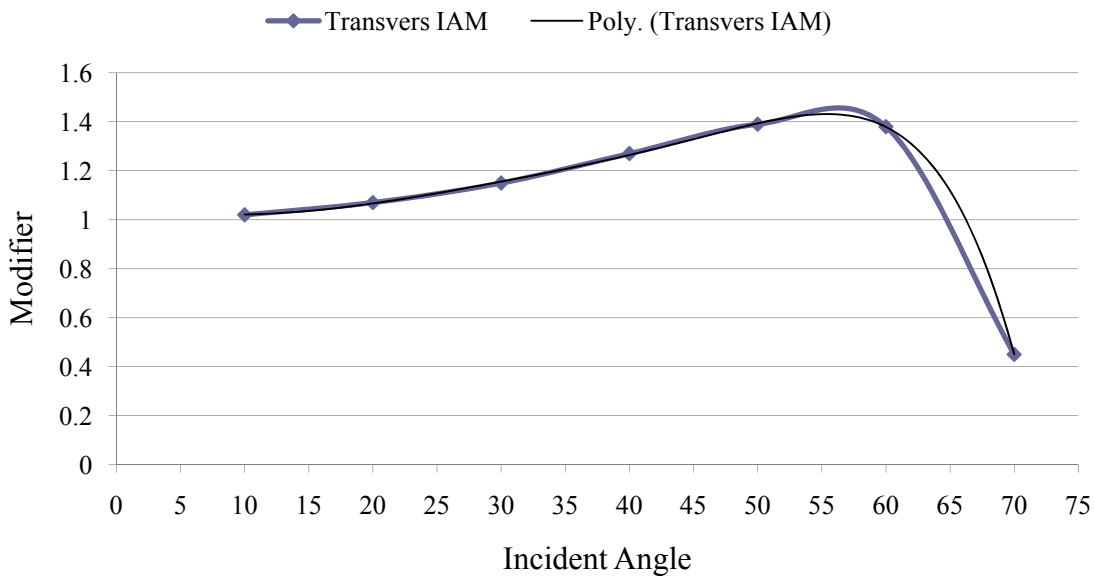

Figure 2.13 Transverse incident angle modifier for different solar incident angles from the SRCC data

Considering $(K_{\tau\alpha})_l$ as unity, the total IAM becomes equal to $(K_{\tau\alpha})_t$ and the total absorbed solar radiation on a tilted collector (Equation 2.4.16) can be modified as (Duffie & Beckman, 2006):

$$S = I_c \times K_{\tau\alpha} \quad (2.4.18)$$

The SRCC also provides the efficiency equation for different collectors from experimental data which relates the ratio of thermal energy produced by the collector to the solar radiation received by the collector. The equation of efficiency for the collector used in this study is (SRCC, 2011):

$$\eta = 0.483 - 1.05630 \left(\frac{T_i - T_a}{S}\right) - 0.0105 \left(\frac{(T_i - T_a)^2}{S}\right) \qquad (2.4.19)$$

Where T_i is the inlet water temperature to collector, T_a is ambient temperature, and S is the total solar radiation absorbed by collector from the Equation 2.4.18. The efficiency represents the percentage of total solar energy that is converted to useful thermal output. With using the efficiency equation, the useful thermal energy produced by collectors can be derived from following equation:

$$Q_{u,c} = A_c \eta_c S \qquad (2.4.20)$$

Which $Q_{u,c}$ is the useful energy (W), A_c is collector gross area (m^2), η_c is collector efficiency, and S is the total solar radiation absorbed by collector (W/m^2).

The SRCC data are measured for a certain flow rate (0.0207 kg/s m^2) and when a collector is used at a different flow rate, a flow rate modification needs to be applied to the efficiency equation. Because of the nature of the simulation in this study that collector flow rate is one of the parameters used in designing the solar absorption cooling system, so this correction factor needs to be considered. Changing the flow rate affects the temperature gradient in the flow direction which changes the collector efficiency factor and consequently the slope of the efficiency to $(T_i - T_a)/G$ line changes, Figure 2.14.

The equation which describes the line in Figure 2.14 can be presented as (Duffie & Beckman, 2006):

$$\eta = \frac{Q_u}{A_c S} = F_R - F_R U_L \left(\frac{(T_i - T_a)^2}{S} \right) \quad (2.4.21)$$

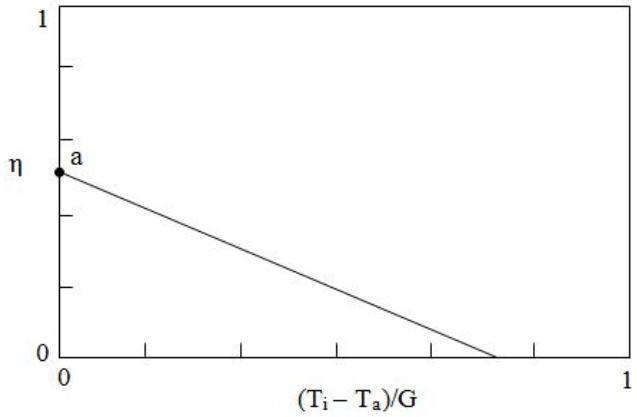

Figure 2.14 Evacuated tube collector efficiency graph

Where F_R is collector heat removal factor and represents an indication of how energy is absorbed and shown as point a in Figure 2.14 which is the intercept of the line of the η axis. U_L is collector overall heat loss coefficient and indicates the energy loss. – $F_R U_L$ is equal to the slope of the line in the plot of η versus $(T_i – T_a)/G$.

Both the interception point and the slope of the line are given by the SRCC in addition to the efficiency equation. For the collector used in this simulation are 0.489 (intercept) and –1.718 W/m^2 °C (slope). From this point, the F_R and $F_R U_L$ need to be corrected by a ratio (r) to represent the effect of changing the flow rate and this ratio is (Duffie & Beckman, 2006):

$$r = \frac{\frac{\dot{m} C_p}{A_c} \left[1 - \exp\left(\frac{- A_c F' U_L}{\dot{m} C_p} \right) \right]_{use}}{F_R U_L|_{test}} \quad (2.4.22)$$

$$F' U_L = - \frac{\dot{m} C_p}{A_c} \ln \left(1 - \frac{F_R U_L A_c}{\dot{m} C_p} \right) \quad (2.4.23)$$

So the modified slope and the intercept point can be calculated as:

$$F_{R,use} = r\, F_{R,test} \tag{2.4.24}$$

$$F_R\, U_{L,use} = r\, F_R\, U_{L,test} \tag{2.4.25}$$

The flow rate correction factor (r) for the current solar absorption cooling system is found to be between 0.995 and 1.02 from the simulation. This factor is considered as unity for further simulations, which means the efficiency profile is considered as equal to equation 2.4.19.

CHAPTER 3 – SIMULATION AND RESULTS

3.1 Absorption System Performance

To model the absorption system, the following assumptions are considered:

- The system is under steady-state conditions.
- It works under full load 24 hours a day.
- The system will turn off when ambient temperatures drop below 20°C.
- The pressure in the evaporator is equal to the pressure in the absorber.
- The pressure in the generator is equal to the pressure in the condenser.
- There is no pressure drop or heat loss in the pipes.
- All the throttling valves are isenthalpic ($h_8 = h_9$).
- All the pumps are adiabatic ($T_1 = T_2$)
- Refrigerant vapor leaving the generator is a high pressure saturated condition.
- Refrigerant vapor leaving the evaporator is low pressure saturated pure liquid.
- Saturated high pressure liquid refrigerant leaves the condenser.
- The strong solution leaving the absorber is saturated at the ambient temperature ($T_1 = T_{amb}$).
- The weak solution leaving the generator is at the saturated condition at the generator temperature ($T_4 = T_g$).
- Refrigerant vapor leaving the generator has the equilibrium temperature of the strong solution at the generator pressure with $T_4 = T_7 = T_g$.
- Condenser and absorber temperatures are equal to the ambient temperature ($T_c = T_a = T_{amb}$).

- Temperature of the chilled water leaving the evaporator is 7°C (T_e).
- The required cooling load is 1 ton (3024 kcal/hr).
- The effectiveness of liquid-liquid heat exchangers is 0.8 (ε_L), between the absorber and the generator and inside the generator.

Crystallization is one of the design points that needs to be considered. The concentration of lithium-bromide (Li-Br) in the weak and strong solutions at different temperatures are simulated and shown in Figures 3.1 and 3.2, respectively. Figure 3.1 shows the concentration of Li-Br in a weak solution, which decreases with increasing the ambient temperature at constant generator temperature. Figure 3.2 demonstrates the concentration of Li-Br in a strong solution (high refrigerant solution), which increases by increasing the ambient temperature at constant generator temperature.

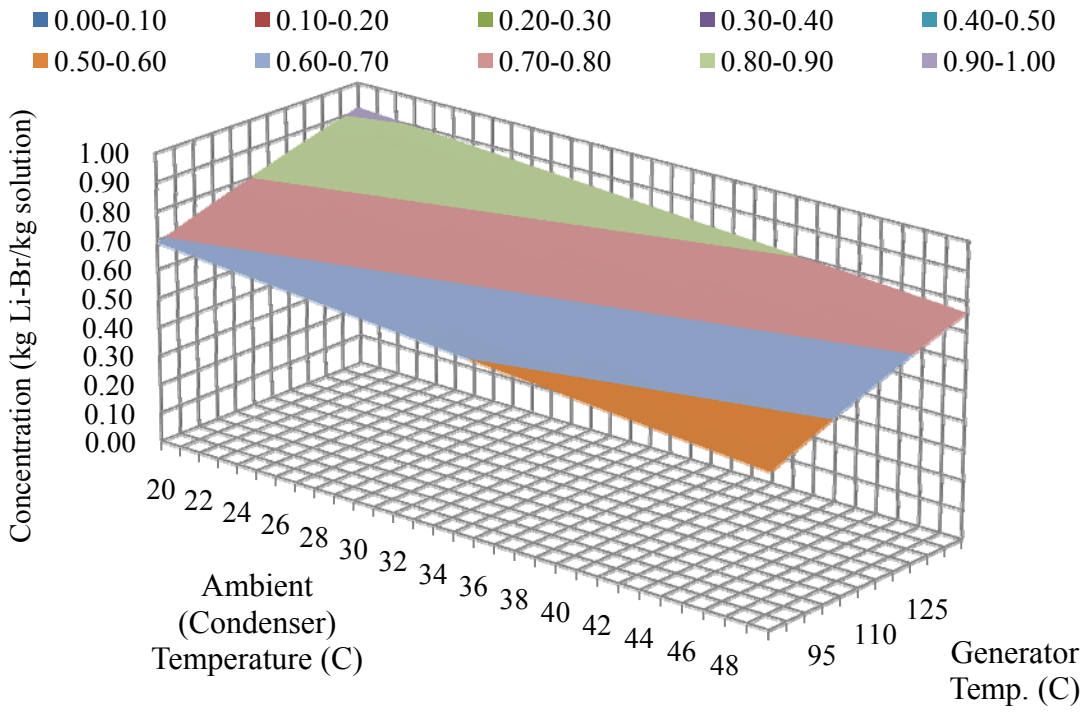

Figure 3.1 Weak solution concentration (X4) versus ambient temperature at different generator temperatures.

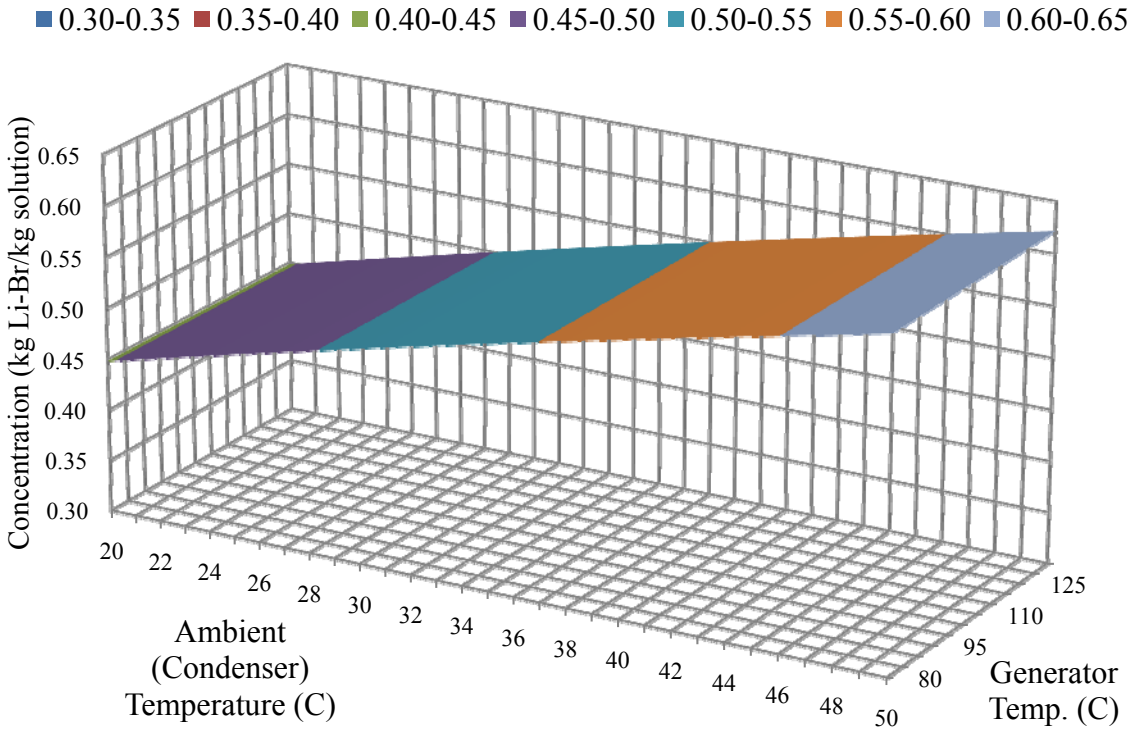

Figure 3.2 Strong solution concentration (X1) versus ambient temperature at different generator temperatures.

According to ASHRAE (1997), the amount of concentration of lithium bromide in solution must be less than 70% to avoid formation of salt crystals and more than 40% to absorb water in the absorber. The probability of dropping the concentration below 40% is at the strong of refrigerant solution line (stage 1 to 3) and above 70% is at the weak solution line (stage 4 to 6). The concentration of Li-Br in strong solution is dependent on the absorber temperature and the evaporative temperature. Because the evaporative temperature is constant, the absorber temperature, which is equal to the ambient temperature, affects the strong solution concentration.

Figure 3.3 shows the concentration of weak and strong solutions at 45°C ambient temperature, which is maximum ambient temperature in the cooling season in Las Vegas.

The concentration in a strong solution stays constant for different generator temperatures because the ambient (absorber) temperature doesn't change.

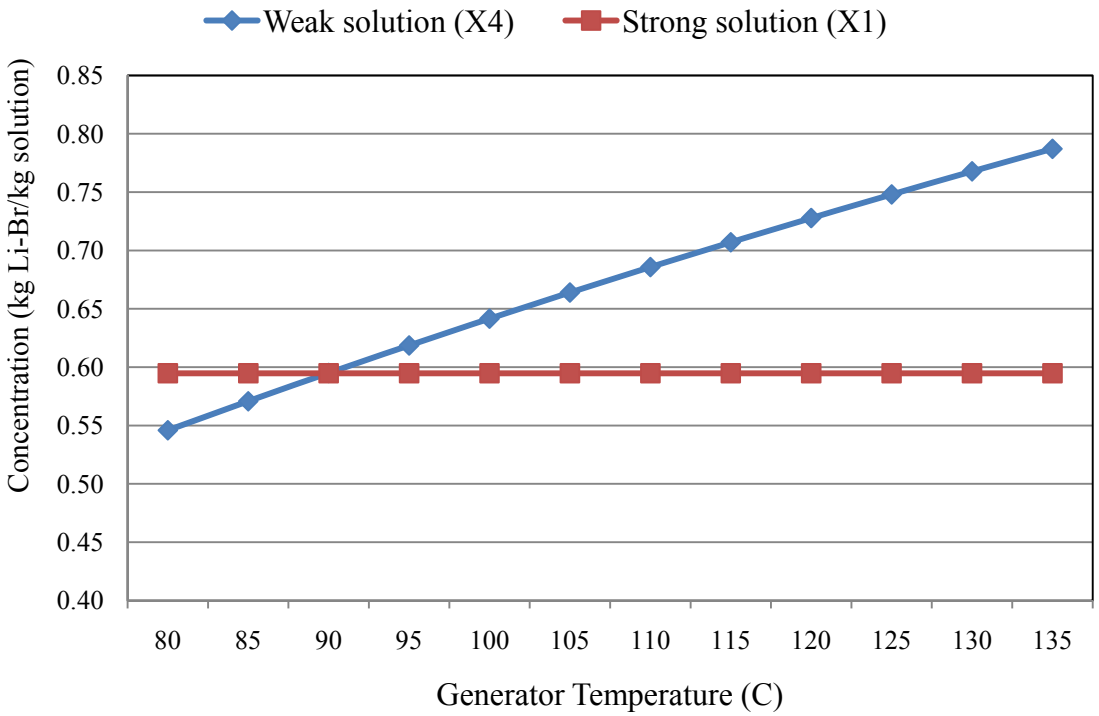

Figure 3.3 Concentration of Li-Br in solution at a 45 °C ambient temperature.

The concentration of Li-Br in a strong solution is dependent on both the generator temperature and the condenser temperatures. Under constant condenser temperature (ambient), the higher generator temperature causes an increase in concentration. Figure 3.4 shows the effect of ambient temperature on strong and weak solution concentrations at constant generator temperature (105°C). With increasing the ambient temperature, the concentration in a strong solution decreases, while the concentration in a weak solution increases.

When the concentration between the weak and strong solutions become close together, the absorption system stops working because there is very little driving force for concentration exchange in the generator refrigerant.

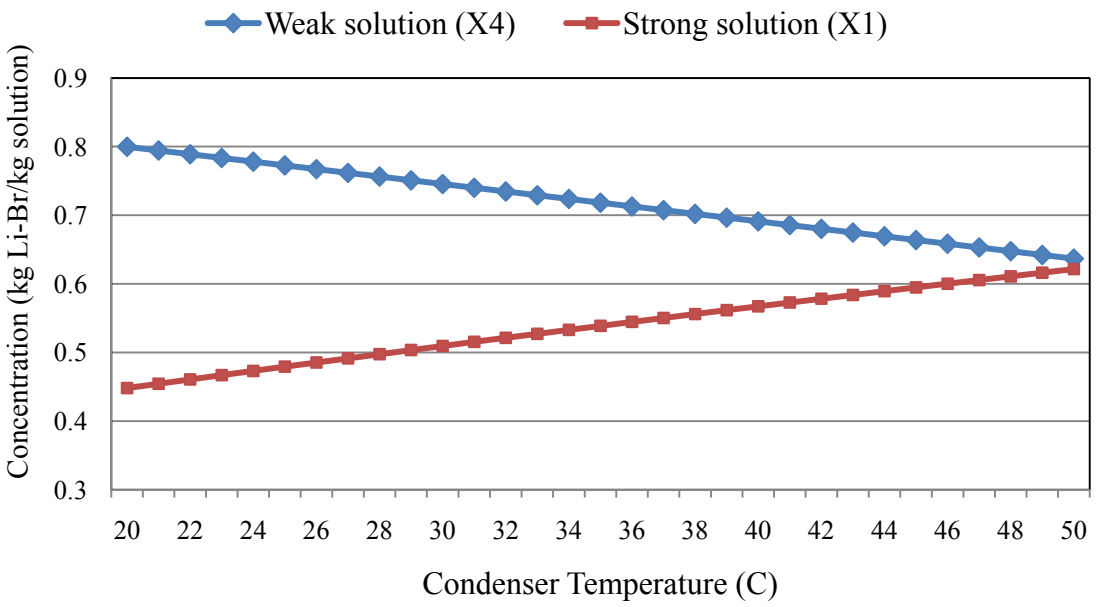

Figure 3.4 Concentration of Li-Br in solution at 105°C generator temperature.

The refrigerant flow rate is dependent on the cooling load, the evaporator temperature and the condenser temperature. In this simulation, the cooling load (1 ton) and the evaporator temperature (7°C) are constant. As seen in Figure 3.5, the condenser temperature is the only parameter which affects the refrigerant (water) flow rate.

At constant generator temperatures, the water flow rate increases by increasing the ambient temperature. But at constant ambient temperature, which is assumed to be the condenser temperature in this analysis, the water flow rate stays the same at different generator temperatures. Generally, the water flow rate changes are small and can be taken to be a constant during the cooling season in Las Vegas.

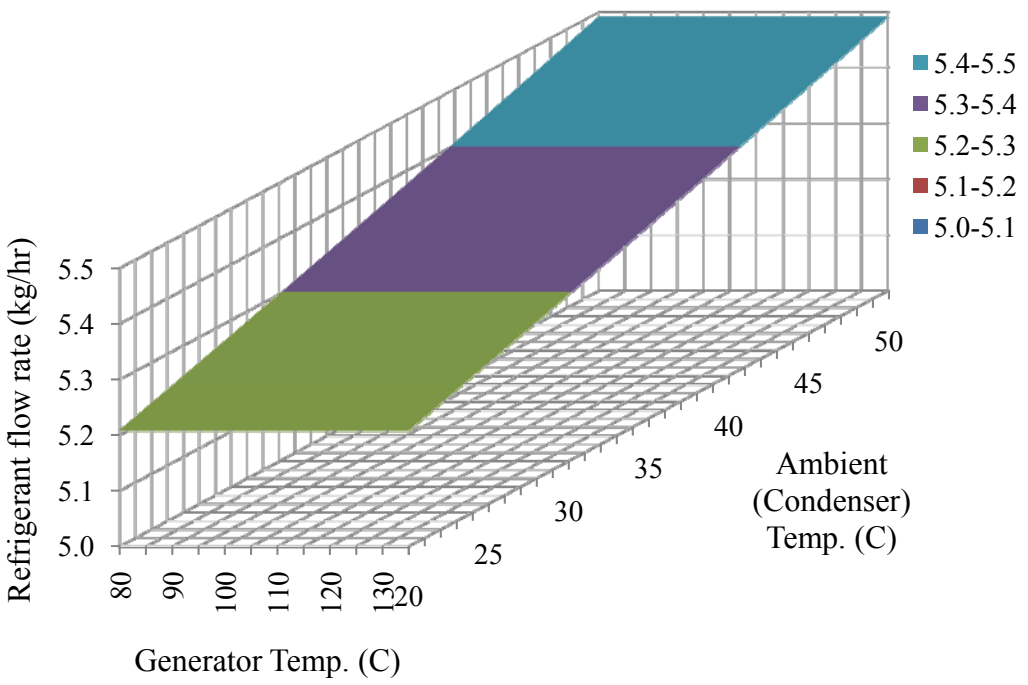

Figure 3.5 Refrigerant flow rate versus ambient temperature for different generator temperatures.

A strong solution flow rate is dependent on strong and weak solution concentrations. Figure 3.6 shows the strong solution concentration with changing the ambient temperature at different generator temperatures. As seen in this graph, the flow rate at some points becomes very large or negative. The large or negative flow rates in reality never happen because at those conditions, the concentration of the strong solution approaching the weak solution and the potential for any mass transfer is minimized. Consequently, the system stops working.

When considering a control point for concentration, while omitting the possibilities of concentrations more than 70% or less than 40%, the modified strong solution flow rate variation is as shown in Figure 3.7. This figure shows that the flow rate at high ambient temperature and low generator temperature is zero and the system goes

off. Generally, at constant generator temperature, the strong solution flow rate decreases by increasing the ambient temperature.

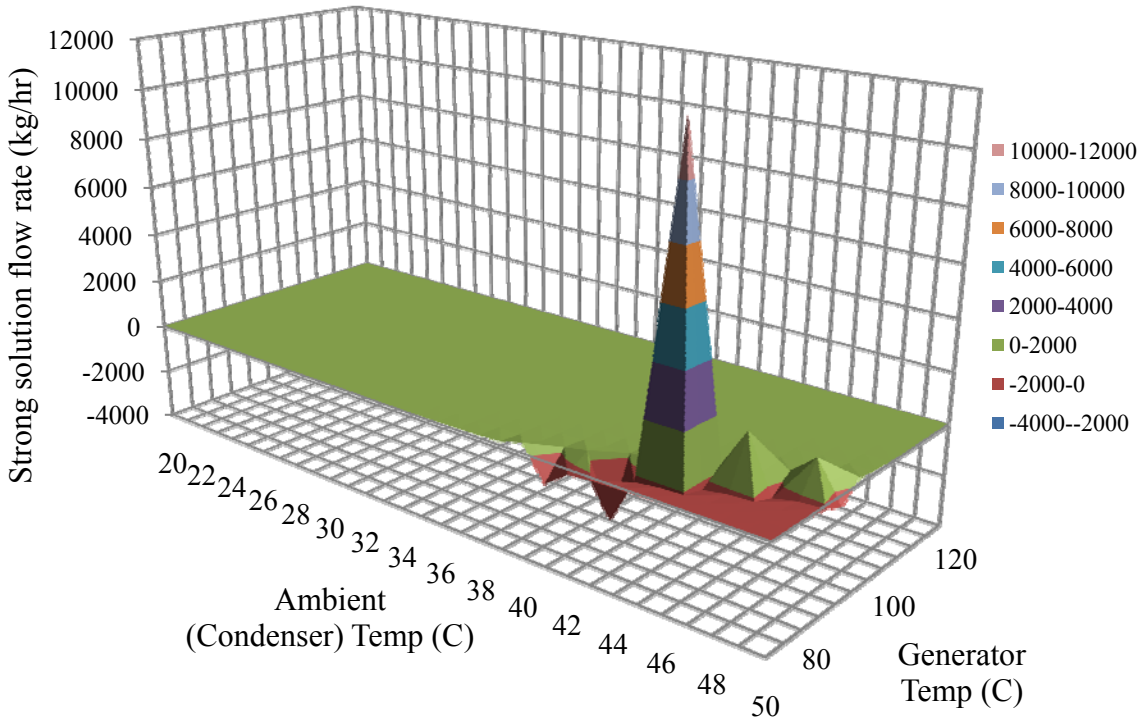

Figure 3.6 Strong solution flow rate versus ambient temperature at different generator temperatures.

Generally, at constant ambient temperature, there are different choices for selecting the generator temperature to achieve a good strong solution flow rate, and this flow rate can be used as a control point. When flow rate is set to 50 kg/hr and the generator temperature is 105°C, the ambient temperature needs to be 45°C, as shown in Figure 3.8.

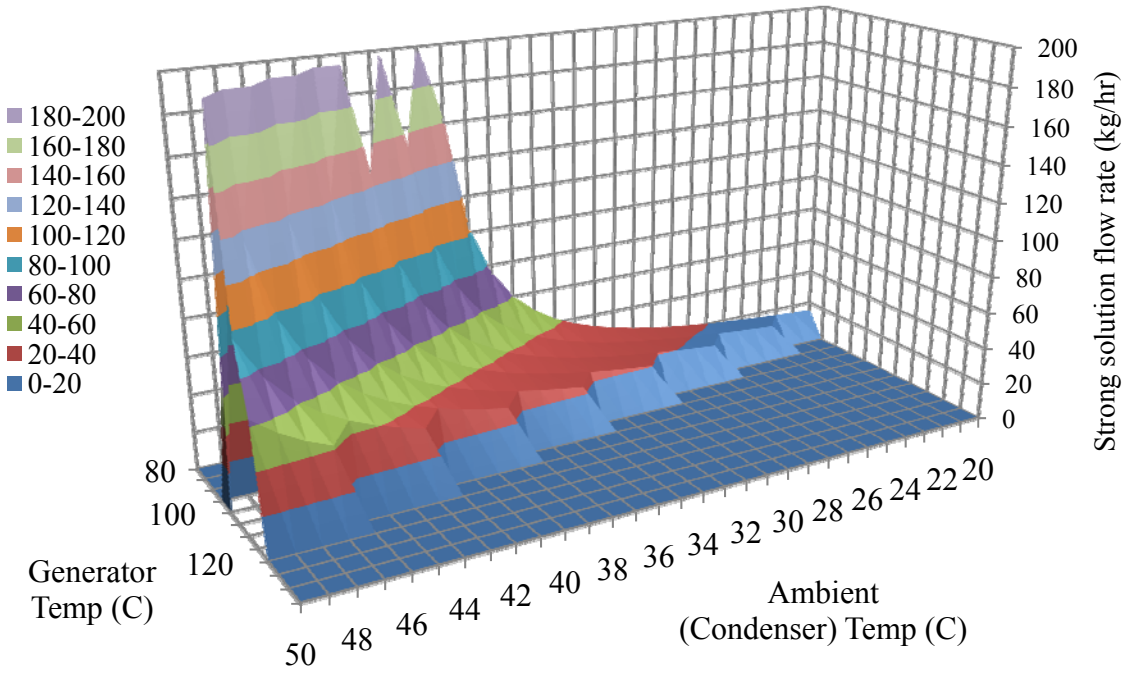

Figure 3.7 Strong solution flow rates using concentration control

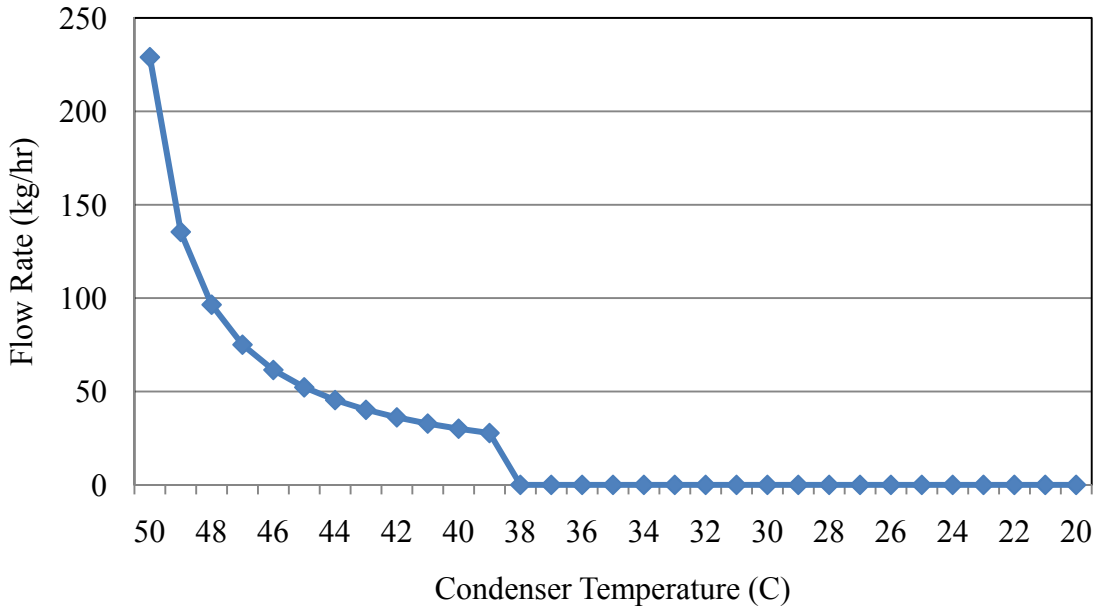

Figure 3.8 Strong solution flow rates at 105 °C generator temperature

The amount of heat used by the generator in an absorption system is dependent on the generator, the evaporator, the condenser and the absorber temperatures. Since T_e is constant and $T_a = T_c = T_{amb}$, this energy becomes related to the ambient temperature and the generator temperature, as shown in Figure 3.9. At certain ambient temperatures, the amount of required energy decreases by increasing the generator temperature. The graph illustrates some nonuniform pattern under condition of high ambient and low generator temperatures. Under these conditions, the concentration is out of the design range (40% < X_1 & X_4 <70%), consequently the system practically doesn't work.

Figure 3.10 shows both the energy required by the generator and the weak/strong solution concentrations for different ambient temperatures, at a fixed generator temperature of 90°C. This graph defines a decrease in generator energy for ambient temperatures higher than 44°C, which are out of the design range. The system doesn't work under these conditions.

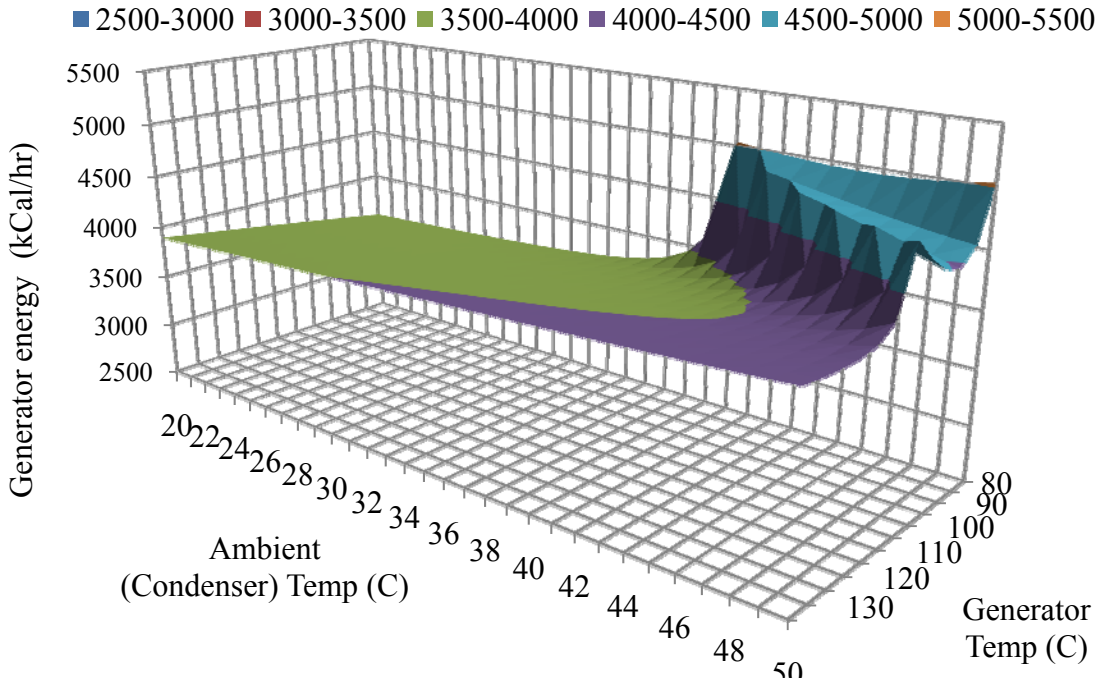

Figure 3.9 Energy required by generator versus ambient temperature at different generator temperatures

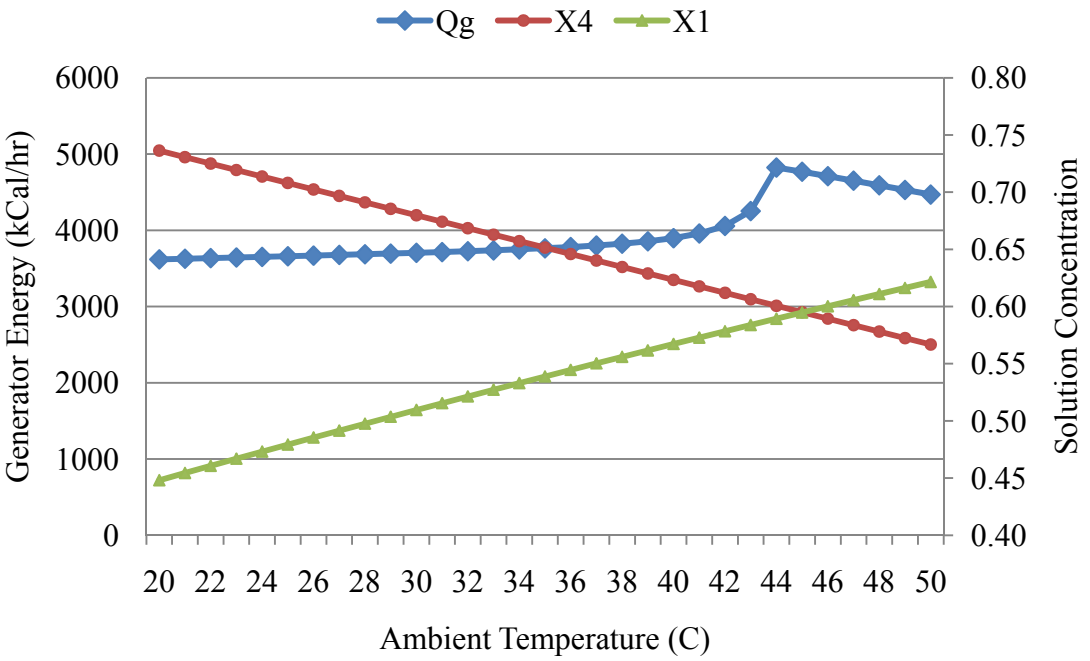

Figure 3.10 Required generator energy and concentrations versus ambient temperature at T_g = 90 °C

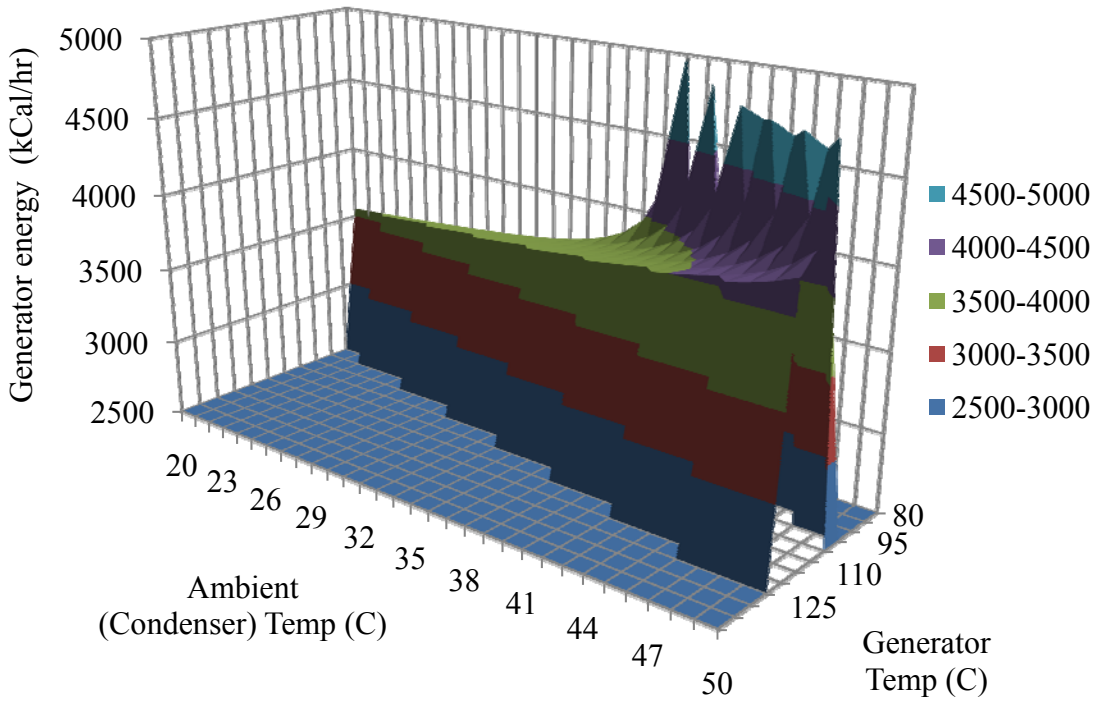

Figure 3.11 Modified generator energy requirement versus ambient temperature at different generator temperatures

Taking to the account the concentration factor, the heat required by the generator can be modified as shown in Figure 3.11. It can be deduced that at particular generator temperatures, the heat required by the generator increases with increasing ambient temperature.

The coefficient of performance (COP) for the absorption cooling system is dependent on the generator energy and the cooling load (the pump work is small and can be neglected). The cooling load is constant so the COP becomes related to the generator heat usage, which is related to the ambient and the generator temperatures, as shown in Figure 3.12. This graph demonstrates nonuniform behavior at high ambient and low generator temperatures. At these points, the concentrations of the weak and strong solutions are out of the design range, as shown in Figure 3.13.

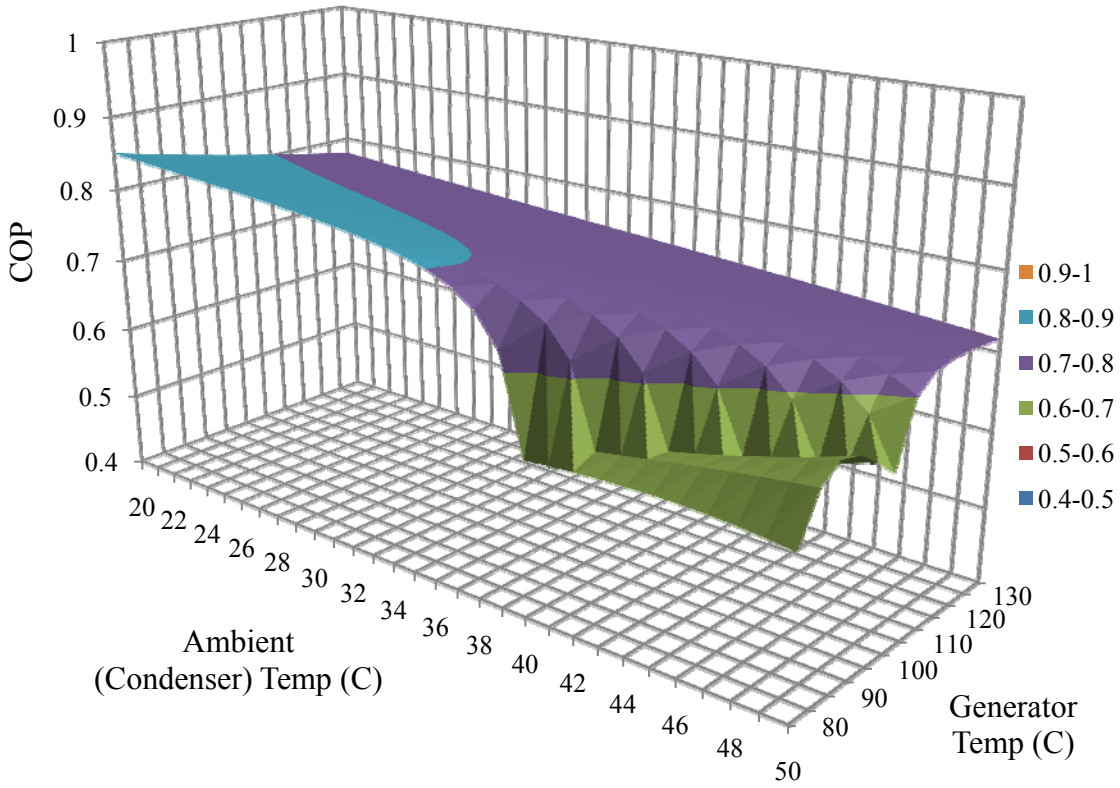

Figure 3.12 Coefficient of performance versus ambient temperature at different generator temperatures

Generally, at constant generator temperature, the coefficient of performance reduces with increasing the ambient temperature, as shown in Figure 3.13. Also, at certain ambient temperatures, there is a corresponding generator temperature which produces the highest COP, as shown in Figure 3.14. At a 45°C ambient temperature for example, the corresponding generator temperature is 105°C for the maximum COP.

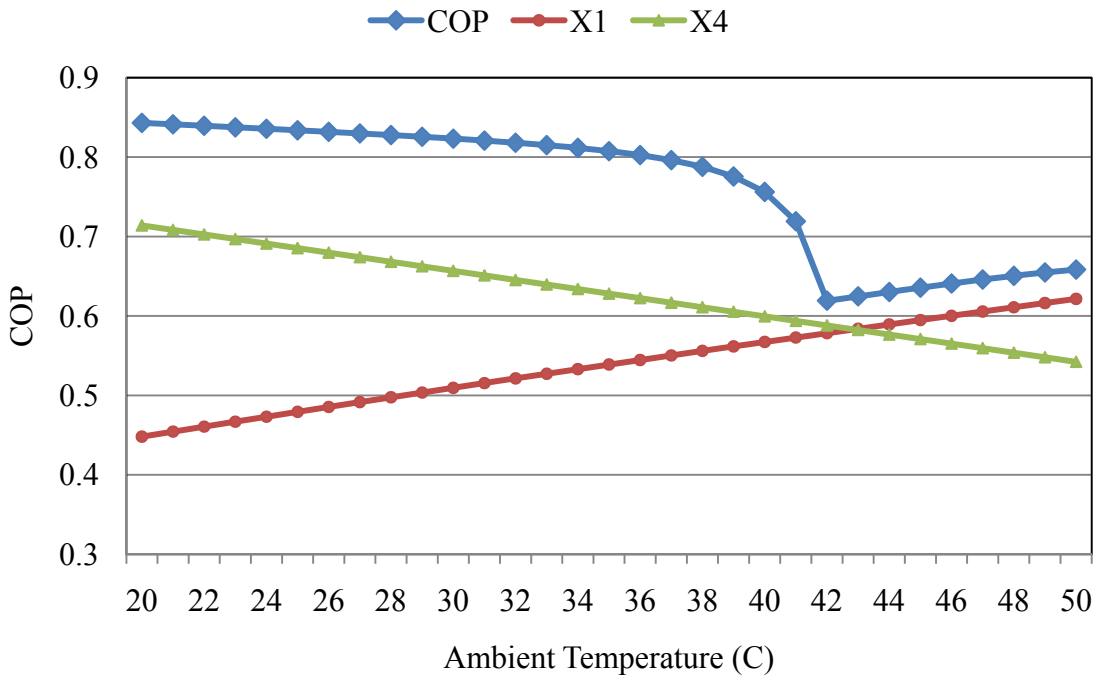

Figure 3.13 COP and concentrations versus ambient temperature at an 85 °C generator temperature

With combination of various control criteria, such as concentrations ($40\% < X_1$ & $X_4 < 70\%$), difference between concentration ($0.04 < |X_1 - X_4| < 0.2$), and maximum COP, the desired generator temperature can be calculated. Figure 3.15 demonstrates the effect of these control points on selecting the generator temperature at different ambient temperatures. For the ambient temperatures between 20°C to 35°C, the generator temperature of 80°C is suitable. For each 2°C increase in the ambient temperature beyond 80°C, the generator temperature needs to be increased by 5°C.

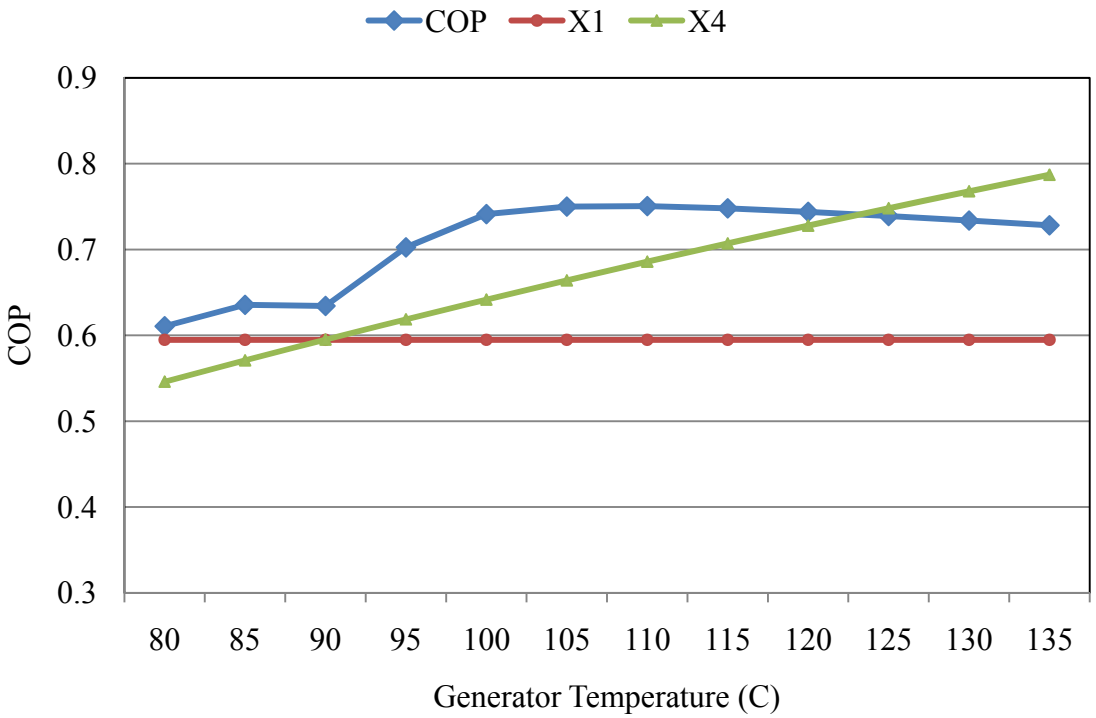

Figure 3.14 COP and concentrations versus generator temperature at a 45 °C ambient temperature

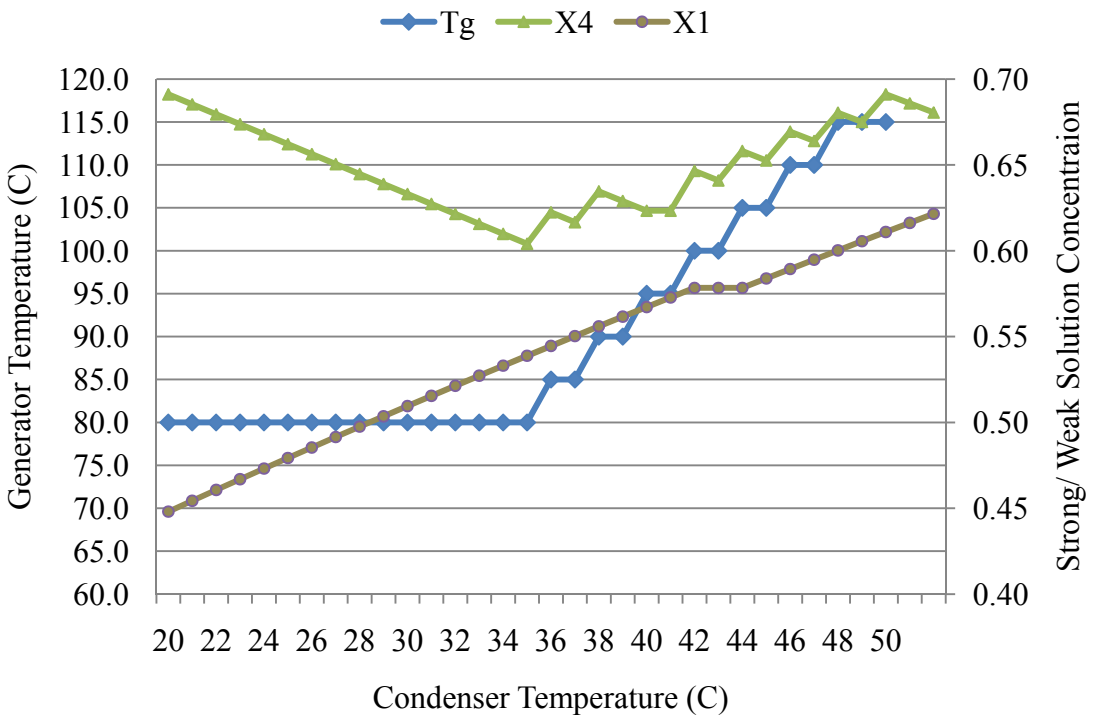

Figure 3.15 Generator temperature and solution concentrations at different ambient temperatures

The maximum generator temperature is 115°C. For higher temperatures the concentration of the strong solution exceeds 70% and crystallization occurs. Figure 3.16 demonstrates a reduction in COP with increasing the ambient temperature, even with an increase in the generator temperature.

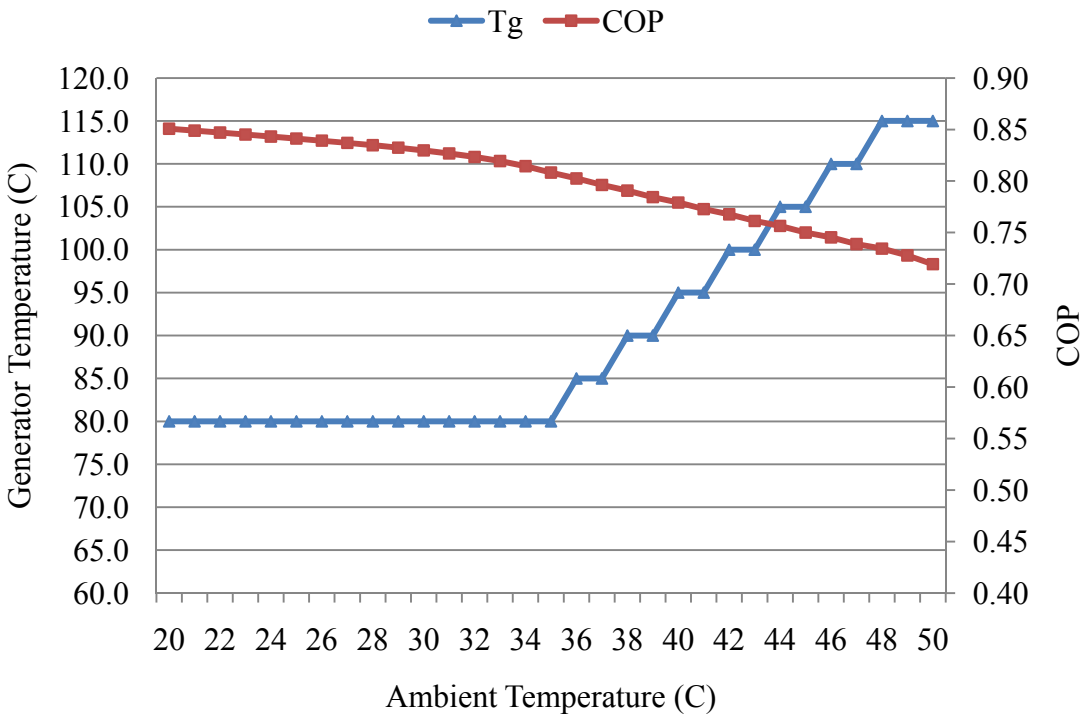

Figure 3.16 Generator temperature and COP for different ambient temperature

Figure 3.17 shows the effect of selecting appropriate generator temperatures on the strong solution flow rate at different ambient temperatures. So Figure 3.6 can be modified as Figure 3.17, by using appropriate control strategies. This graph demonstrates that the solution flow rate is limited between 10 and 70 kg/hr.

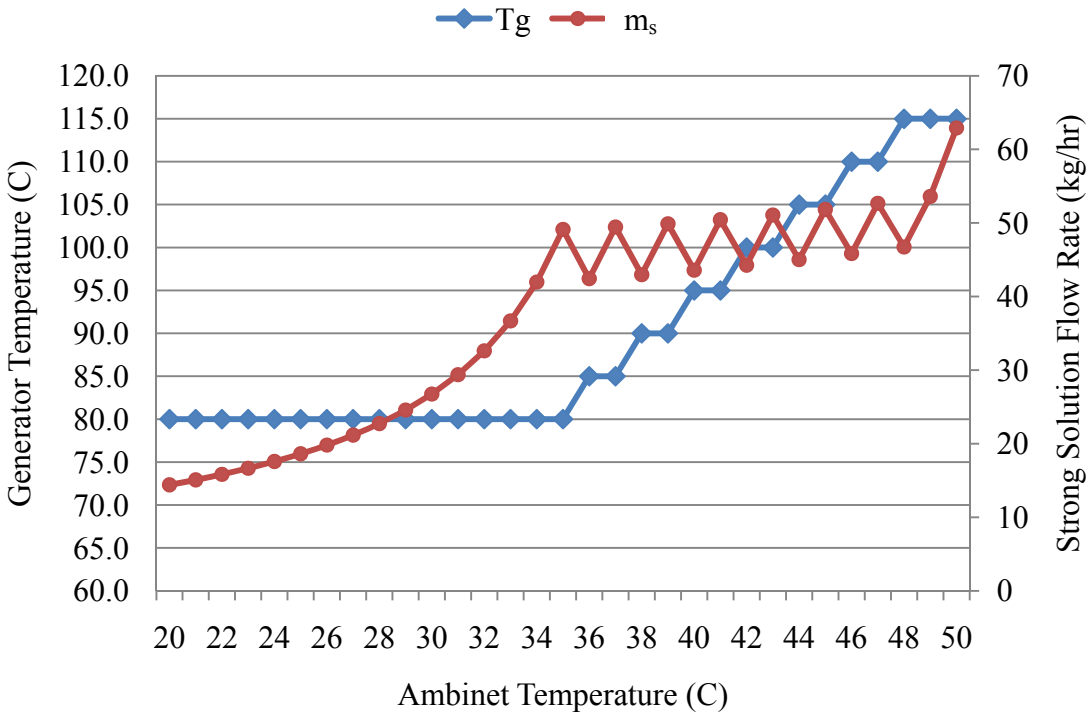

Figure 3.17 Generator temperature and weak solution flow rate at different ambient temperatures

3.2 Solar Radiation

Total solar radiation on a collector surface is related to tilt angle (Σ) and collector azimuth angle (ϕ_c). The collector direction is assumed to be south facing ($\phi_c = 0$) and the collector tilt angle needs to be selected. Tilting the collector horizontally gives the highest absorbed solar radiation in summer but lowest in winter. Conversely, orienting the collector vertically provides the highest absorbed solar radiation in winter. To produce constant energy throughout the year, the collector should be tilted at an angle equal to the latitude of the site. The effect of different tilt angle on monthly solar radiation is shown in Figure 3.18. Considering that the cooling season is from April to September, the tilt angle of Latitude – 15 provides the best distribution of solar radiation. The Las Vegas latitude

is 36.1° and fixing the collector at 21.1° gives almost the uniform average monthly solar radiation during the cooling season.

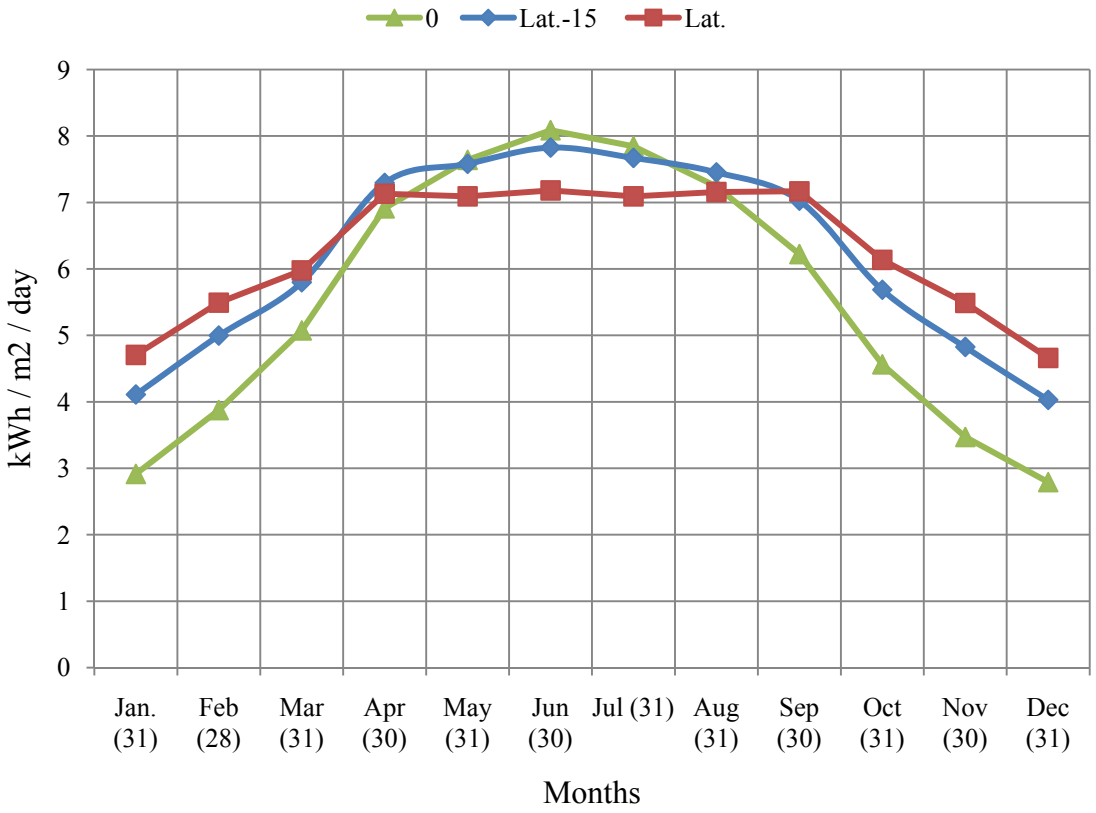

Figure 3.18 Average monthly solar radiation for different tilt angles

Figure 3.19 demonstrates the average monthly solar radiation in Las Vegas for a tilt angle of latitude – 15. This graph shows a good match between the Redbook data (Marion & Wilcox, 1994) and the simulation of average monthly radiation using TMY3 hourly data, (Equation 2.4.10, and Equations 2.4.13 through 2.4.15, which are indicated in chapter 2).

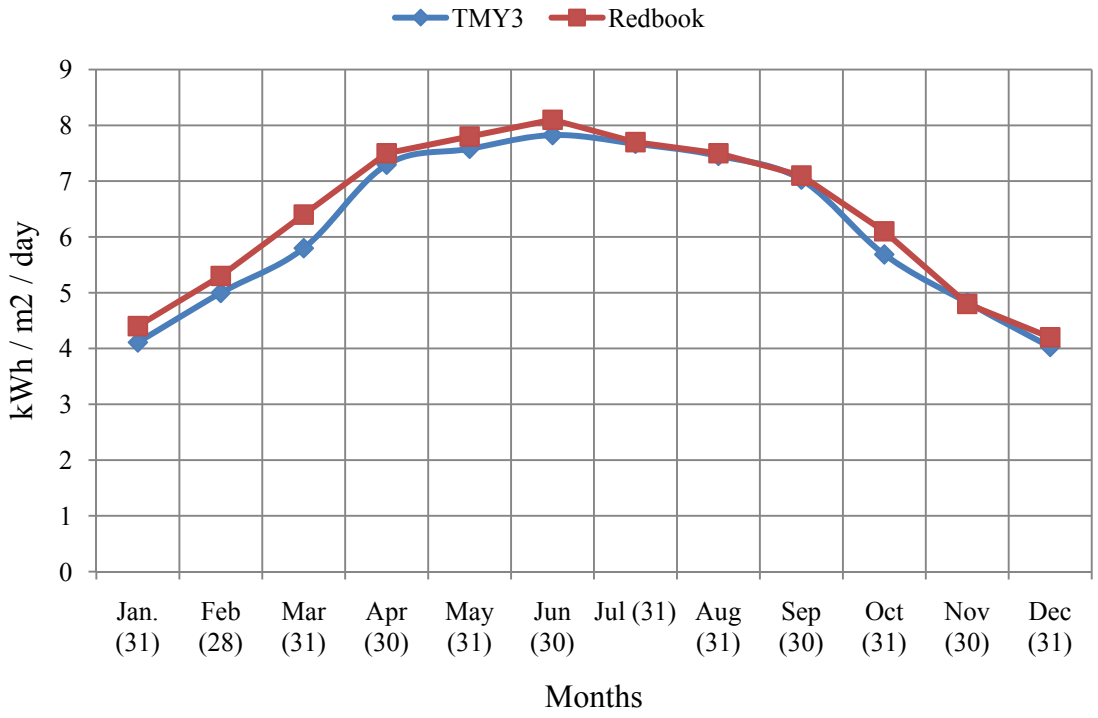

Figure 3.19 Average monthly solar radiations for tilt angle of Latitude – 15 in Las Vegas

3.3 Solar Absorption Cooling System Performance

Different approaches need to be considered to size the collector area in the solar absorption cooling system: for instance, the maximum energy required in the generator, the maximum ambient temperature, the maximum hourly solar radiation, the minimum collector efficiency, etc. For this simulation, the maximum ambient temperature is selected as the design point, which means the solar radiation and energy required in generator are related to the hottest hour during the cooling season. The maximum ambient temperature in Las Vegas according to TMY3 data is 44.4°C which occurs on 4th of June at 3PM. The related total solar radiation is 785.4 W/m^2 and the generator temperature is 105° according to Figure 3.15. The power required by the generator to

provide 1 ton of cooling during this hour is 4.66 kW. This energy needs to be furnished by collectors during this hour.

As mentioned in Chapter 2, the SolarUS SL-30 collector efficiency and the incident angle modifier (IAM) can be calculated from the SRCC data sheet. The total heat production by one unit of collector for this hour is:

$$Q_{u,c} = A_c \, \eta_c \, K_{\tau\alpha} \, I_c \tag{3.3.1}$$

$$= 3.057 \text{ m}^2 \times 0.3411 \times 1.39 \times 785.44 \text{ W} = 1138.42 \text{ W}$$

And the total number of collectors to provide desire heat on the generator becomes:

$$N = \frac{\text{Energy required in the generator}}{\text{Energy produced by one collector}} = 4.1 \text{ unit} \tag{3.3.2}$$

By considering 4 collectors on the simulation, the total energy furnished by the solar radiation can be shown in Figure 3.20.

Solar energy production is generally higher than generator requirement, which comes from the collector tilt angle and the design criteria used. The maximum ambient temperature is selected as the design criteria but the solar radiation at that time is not the maximum amount for the season. This implies that the collector will produce more energy than required for the times that solar radiation is higher than 785.4 W. One way to save this energy is by using hot storage, which is not covered in this study. The other way is to change the water flow rate to the collector by using a variable speed pump.

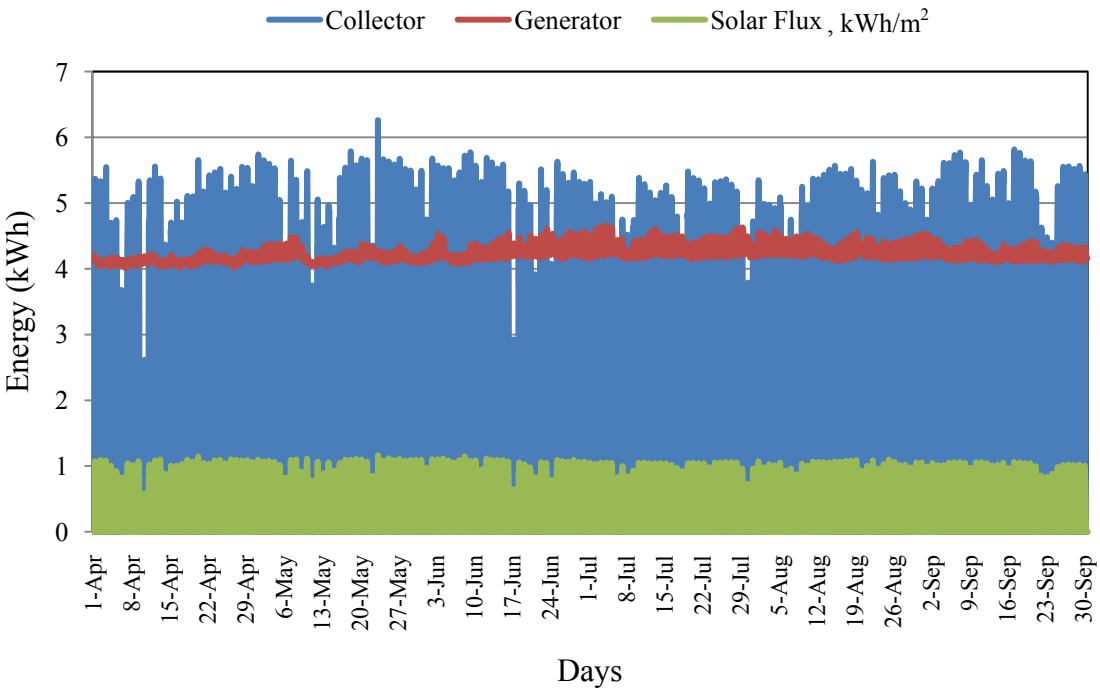

Figure 3.20 Total energy produced by collectors, energy needed by generator, and total solar radiation during the cooling season in Las Vegas

Figure 3.21 illustrates the collector energy production and the generator energy requirement during the first week of June. The collector provides reasonable heat for the absorption cooling system during most of the day. However the system works continuously so during night time or cloudy conditions, an auxiliary heat source is required

Figure 3.22 demonstrates the absorption system behavior during the first week of June. The ambient temperature is normalized by dividing it by the maximum ambient temperature which is 44.4°C and occurs on June 4th at 3PM. The strong and weak solution concentrations are in the safe zone, which shows the control approach (like changing the generator temperature) works well. By increasing the ambient temperature, the COP of the absorption system decreases and the concentrations of weak and strong solution increase.

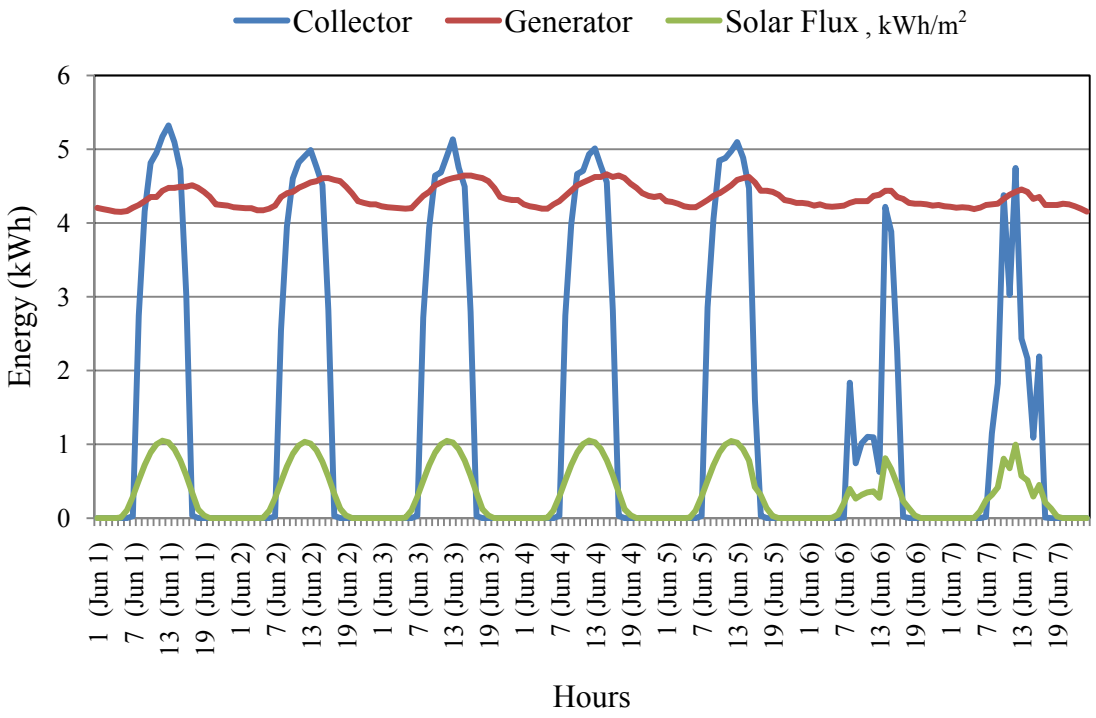

Figure 3.21 Collector energy, generator required energy and solar radiation in the first week of June

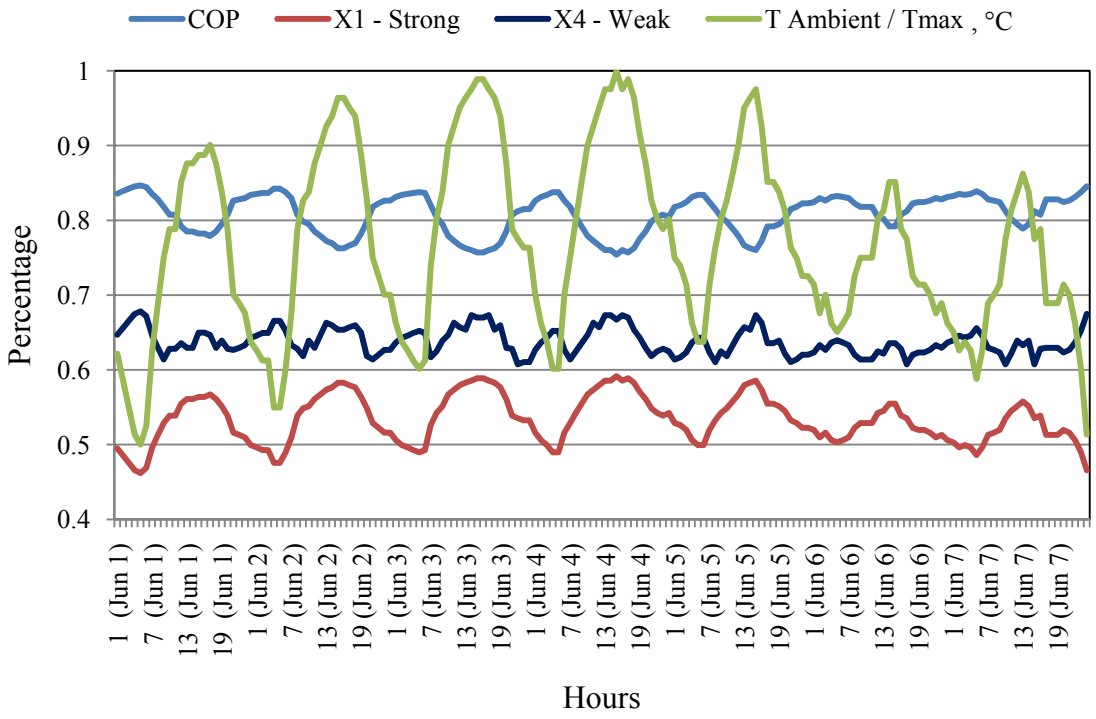

Figure 3.22 COP, solution concentrations, and normalized ambient temperature for the first week of June

It is assumed that the absorption cooling system turns off when the ambient temperature drops below 20°C and also there is excess heat produced by the collector. The auxiliary heat source turns on when the solar energy is not enough to maintain the generator temperature. Figure 3.23 shows the energy consumption and production during the cooling season. The maximum cooling demand happens in month of July. The average energy production from the solar collector is 35% of the energy demand.

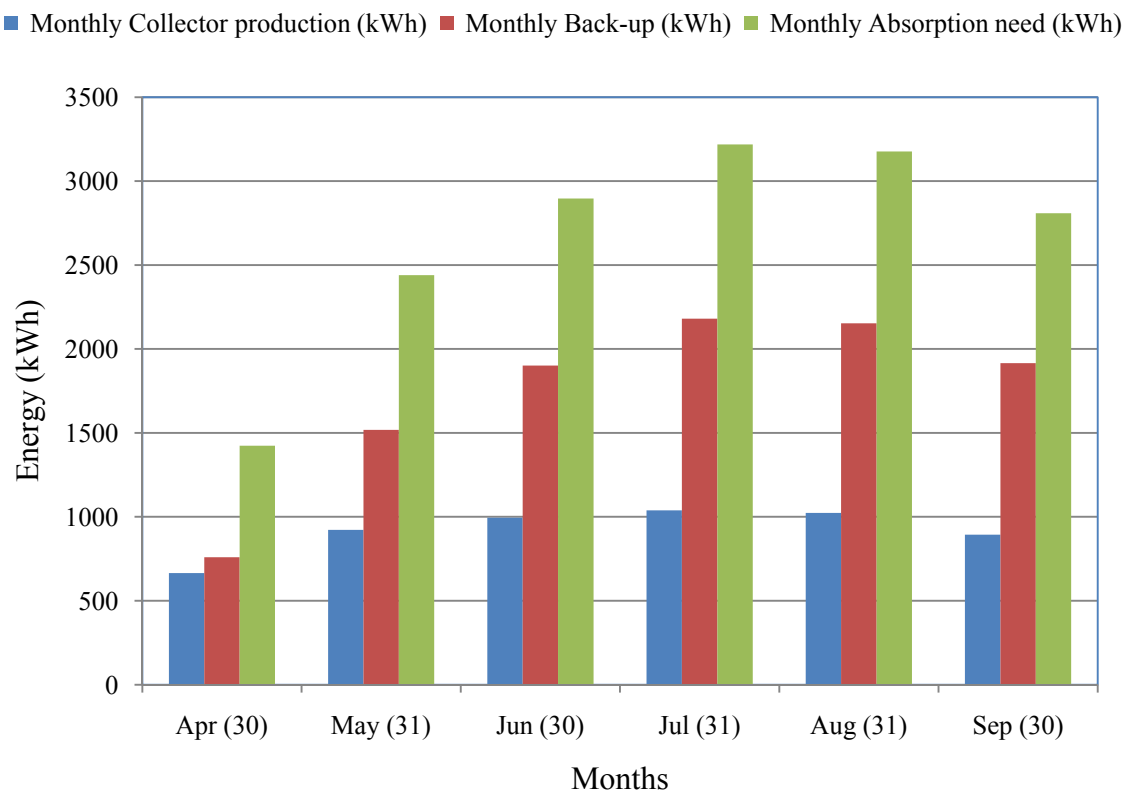

Figure 3.23 Average monthly solar energy production, auxiliary usage, and the generator heat requirement

The temperature difference between inlet and outlet of collector ($\Delta T = T_{coll,out} - T_{coll,in}$) can affect the amount of energy delivered to the generator. By increasing the temperature difference, the flow rate to the collector needs to be reduced because the

amount of energy delivered to the generator is constant. Figure 3.24 shows the effect of various collector temperature differences (ΔT) on flow rate. A temperature difference of 10°C seems to be a good choice for running the collector system.

Also, as explained before, the flow rate correction factor is related to the collector flow rate. Since the flow rate fluctuations are not large, this correction factor can be assumed to be unity. As such, the correction factor can be neglected for calculating the collector efficiency.

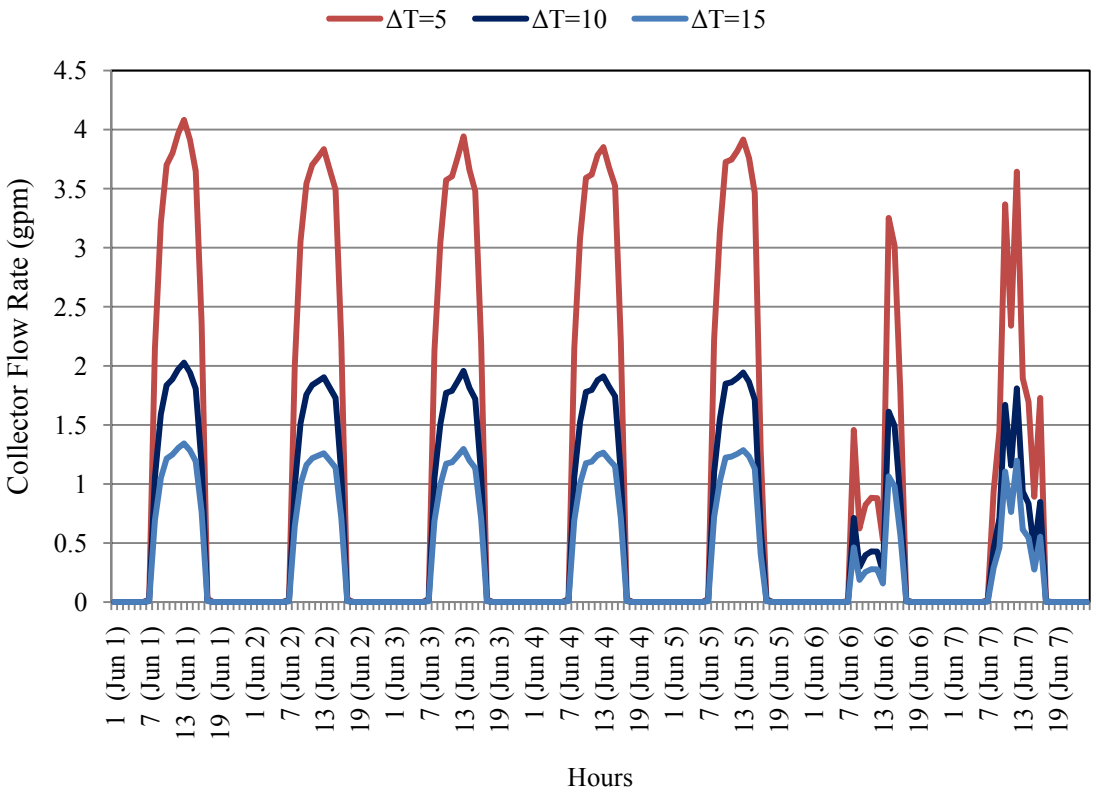

Figure 3.24 Collector flow rates for selective collector temperature's difference (ΔT) at the first week of June

As seen in Figure 3.25, the collector efficiency is negligibly affected by the ΔT and it is found that the efficiency equation given by the SRCC can be used without any modification.

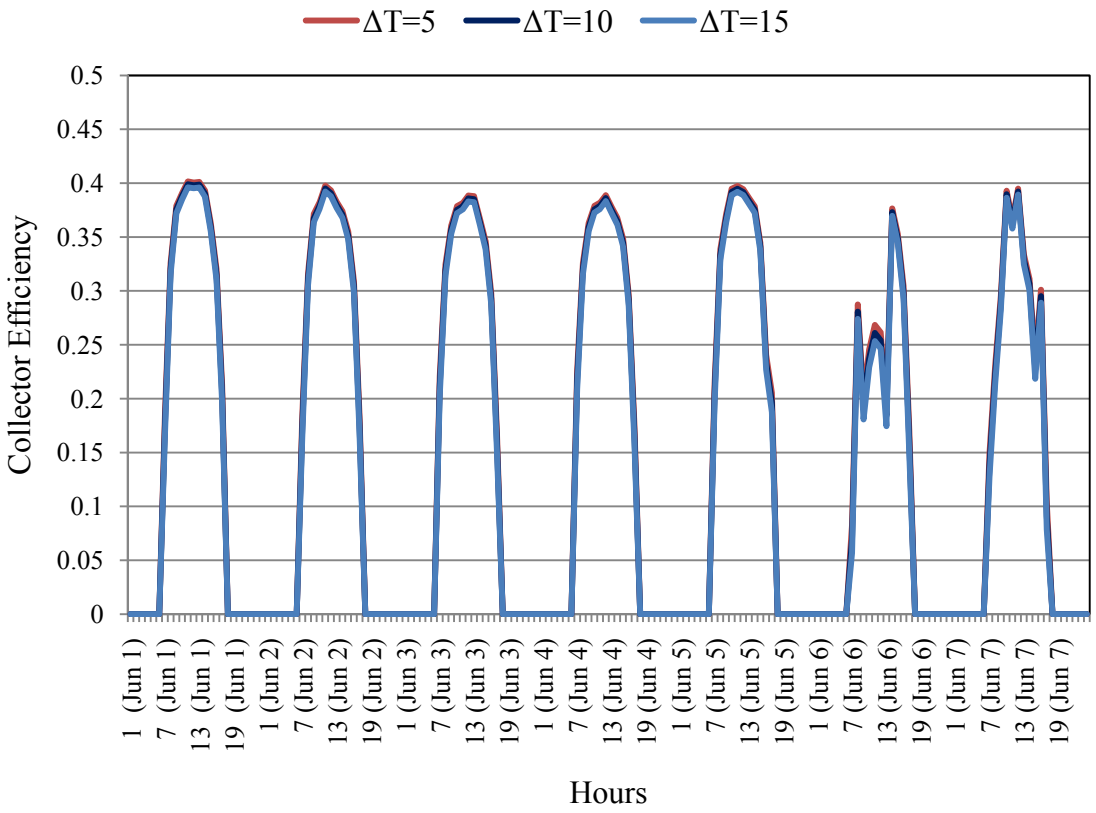

Figure 3.25 Collector efficiency for various temperature differences (ΔT_{coll}) during the first week of June

Finally after applying all the control strategies and modification, the solar absorption cooling system works as shown in Figure 3.26, during the cooling season in Las Vegas. For the month of April, the Li-Br solution concentrations sometime go beyond 70% or below 40% due to the ambient temperature getting below 20°C. The system shuts down during those times as was assumed earlier.

The overall coefficient of performance (COP) of the system is approximately 0.8 which is a highly efficient single effect Li-Br/ water absorption cooling system according to ANSI Standard 560 (2000). The 4 south facing collectors at a tilt angle of latitude - 15° provide an average of 35% of the required monthly energy for running this system. The water flow rate in the collector loop and the strong solution flow rate in the absorption

side are controlled by variable speed pumps. These pumps are assumed to be controlled by temperature feedbacks from the condenser, the evaporator, and the generator.

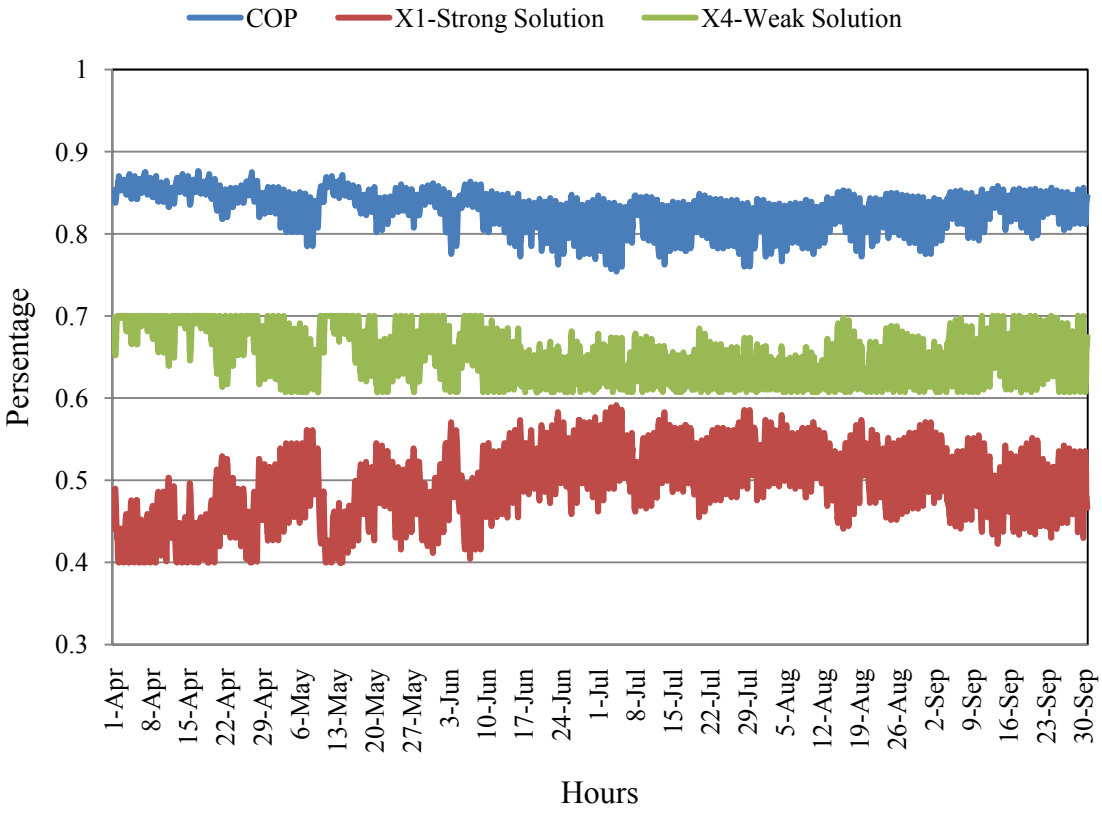

Figure 3.26 COP and concentrations during the cooling season in Las Vegas

Figure 3.27 shows various flow rates in the absorption system during the first week of June. A comparison of this chart with Figure 3.6 shows the effectiveness of the control system on the absorption system performance. By changing the generator temperature accordingly with the different ambient temperature, and using a variable speed pump in collector side, the solar absorption system works at its maximum COP and in the safe Li-Br concentration zone. The refrigerant flow rate is almost constant (5.3 kg/hr) and the strong solution flow rate increases at the higher ambient temperature.

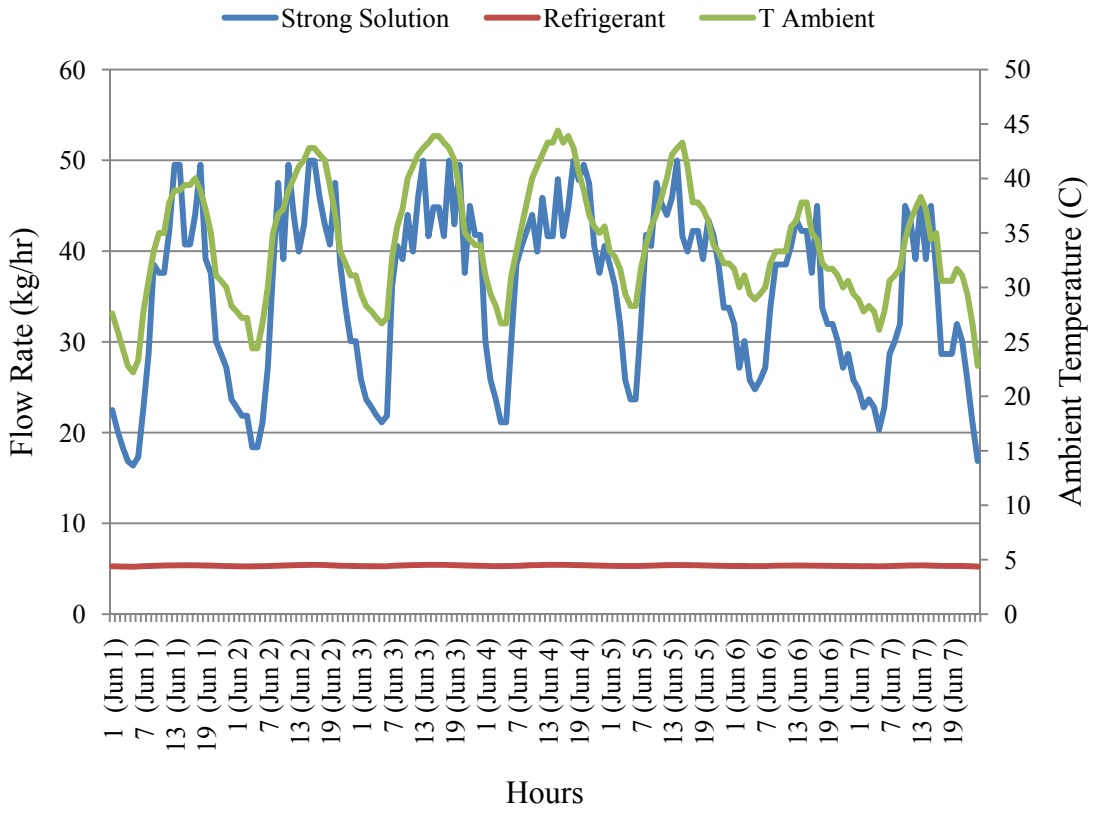

Figure 3.27 Refrigerant flow rate, strong solution flow rate and ambient temperature during the first week of June

CHAPTER 4 – CONCLUSIONS

Conclusions

The current work presents a study that is an assessment of the effect of controlling various parameters on the performance of a single effect solar driven Li-Br absorption cooling system. The condenser and the absorber are assumed to be air cooled, with their temperatures equal to the ambient temperature. Thus, these temperatures cover a wider range compared to a system with a wet cooling tower. Consequently, the inlet generator temperature range is higher. Most absorbent systems with a cooling tower use a flat plate collector, and their generator temperatures are between 65 and 95ºC. This study shows that the air cooled system needs the generator temperature of 85 to 115ºC to maintain the desired cooling demand.

The temperature lift is restricted due to crystallization concerns. This is a control parameter used in this study in designing the absorption system, along with attaining the maximum COP of the system. The simulation shows there is only one inlet generator temperature corresponding to each ambient temperature that produces the highest COP while of keeping the Li-Br concentration in the safe zone.

In this study, the SolarUS, Inc. SL-300 evacuated tube collector is selected and to size the collector area, the maximum ambient temperature during the cooling season in Las Vegas is used (it was 44.4°C on July 4th at 3 PM). When considering the amount of the solar radiation available during this hour and the required heat energy in the generator, the number of collectors is found to be 4. The overall heat supplied by these collectors during the cooling season is found to be 35% of the total energy required by

the absorption system. Finally, the system shows a COP of 0.8 and the strong solution flow rate ranges between 15 to 50 kg/hr.

Recommendation

Several improvements could be made to the solar absorption cooling system simulation in the future. The cooling load of the absorption system is assumed in the model as constant but realistically, the cooling demand will vary depending on the users' temperature setting inside the building and also the ambient temperature. Another improvement to the simulation would be to consider the effect of the heat exchanger inside of each component in the absorption system performance. The type of the heat exchanger and its lay out has tremendous effect in the heat transfer between the ambient temperature and the refrigerant in the condenser, the heating fluid and the solution in the generator, and the chilling water and the refrigerant in the evaporator. Assuming that the dry cooling yields a fluid temperature the same as the ambient is also an assumption that over estimates the performance and could be treated more realistically.

Further investigation within the model can be made with selecting the different design criteria for sizing the collector area. Instead of using the hottest temperature during the day (as used in this study), the maximum solar radiation can be selected to find the total collector area. Another factor that could be considered is to use a tracking collector system.

Most of the commercial buildings and schools work during 9AM to 5PM so reducing the operation time of the absorption cooling system from 24 hours to daytime is another change that can be considered for future studies.

REFERENCES

Agyenim, F., Knight, I., & Rhodes, M. (2010). Design and experimental testing of the performance of an outdoor LiBr/H2O solar thermal absorption cooling system with a cold store. *Solar Energy*, *84*(5), 735–744. doi:10.1016/j.solener.2010.01.013

ANSI Standard 560. (2000). *ANSI standard for absorption water chilling and water heating packages*. Arlington, Virginia.

ASHRAE. (1997). *ASHRAE Handbook- Fundamentals I-P*. Atlanta: American Society of Heating, Refrigerating, and Air-Conditioning Engineers, Inc.

Assilzadeh, F., Kalogirou, S. A., Ali, Y., & Sopian, K. (2005). Simulation and optimization of a LiBr solar absorption cooling system with evacuated tube collectors. *Renewable Energy*, *30*(8), 1141–1159. doi:10.1016/j.renene.2004.09.017

Atmaca, I., & Yigit, A. (2003). Simulation of solar-powered absorption cooling system. *Renewable Energy*, *28*(8), 1277–1293. doi:10.1016/S0960-1481(02)00252-5

Balghouthi, M., Chahbani, M. H., & Guizani, A. (2008). Feasibility of solar absorption air conditioning in Tunisia. *Building and Environment*, *43*(9), 1459–1470. doi:10.1016/j.buildenv.2007.08.003

Choudhury, B., Chatterjee, P. K., & Sarkar, J. P. (2010). Review paper on solar-powered air-conditioning through adsorption route. *Renewable and Sustainable Energy Reviews*, *14*(8), 2189–2195. doi:10.1016/j.rser.2010.03.025

Duffie, J. A., & Beckman, W. A. (2006). *Solar engineering of thermal processes* (3rd ed.). Hoboken, N.J.: Wiley.

Florides, G. A., Kalogirou, S. A., Tassou, S. A., & Wrobel, L. C. (2002). Modelling, simulation and warming impact assessment of a domestic-size absorption solar cooling system. *Applied Thermal Engineering*, *22*(12), 1313–1325.

Herold, K. E., Radermacher, R., & Klein, S. A. (1996). *Absorption chillers and heat pumps*. CRC Press.

Kyoto protocol to the United Nation framework convention on climate change. (1998). Retrieved October 16, 2014, from http://unfccc.int/resource/docs/convkp/kpeng.pdf

Li, Z. F., & Sumathy, K. (2001). Simulation of a solar absorption air conditioning system. *Energy Conversion and Management*, *42*(3), 313–327.

London, A. L. (Alexander L., Kraus, A. D., Shah, R. K., & Metzger, D. E. (1990). *Compact heat exchangers*. New York: Hemisphere Pub. Corp.

Mammoli, A., Vorobieff, P., Barsun, H., Burnett, R., & Fisher, D. (2010). Energetic, economic and environmental performance of a solar-thermal-assisted HVAC system. *Energy and Buildings*, *42*(9), 1524–1535. doi:10.1016/j.enbuild.2010.03.023

Marion, W., & Wilcox, S. (1994). NREL-Solar radiation data manual for flat-plate and concentrating collectors, *463-5607*.

Masters, G. M. (2004). *Renewable and efficient electric power systems*. Hoboken, NJ: John Wiley & Sons.

McIntire, W. R., & Reed, K. A. (1983). Orientational relationships for optically non-symmetric solar collectors. *Solar Energy*, *31*(4), 405–410. doi:10.1016/0038-092X(83)90139-1

Miao, D. (1978). *Simulation model of a single-stage lithium bromide-water absorption cooling unit*. *Lewis Research Center*. Washington, D.C.: National Aeronautics and Space Administration, Scientific and Technical Information Office. Retrieved from http://www.lib.miamioh.edu/multifacet/record/mu3ugb2154899

Nakahara, N., Miyakawa, Y., & Yamamoto, M. (1977). Experimental study on house cooling and heating with solar energy using flat plate collector. *Solar Energy*, *19*(6), 657–662.

Ortiz, M., Barsun, H., He, H., Vorobieff, P., & Mammoli, A. (2010). Modeling of a solar-assisted HVAC system with thermal storage. *Energy and Buildings*, *42*(4), 500–509. doi:10.1016/j.enbuild.2009.10.019

Pongtornkulpanich, A., Thepa, S., Amornkitbamrung, M., & Butcher, C. (2008). Experience with fully operational solar-driven 10-ton LiBr/H2O single-effect absorption cooling system in Thailand. *Renewable Energy*, *33*(5), 943–949. doi:10.1016/j.renene.2007.09.022

Praene, J. P., Marc, O., Lucas, F., & Miranville, F. (2011). Simulation and experimental investigation of solar absorption cooling system in Reunion Island. *Applied Energy*, *88*(3), 831–839. doi:10.1016/j.apenergy.2010.09.016

Rosiek, S., & Batlles, F. J. (2009). Integration of the solar thermal energy in the construction: Analysis of the solar-assisted air-conditioning system installed in CIESOL building. *Renewable Energy*, *34*(6), 1423–1431. doi:10.1016/j.renene.2008.11.021

SRCC. (2011). *SRCC Ratings Report- SolarUS SL_30*. Cocoa, Florida. Retrieved from https://secure.solar-rating.org/Certification/Ratings/RatingsReport.aspx?device=1158&units=METRICS

Syed, A., Izquierdo, M., Rodríguez, P., Maidment, G., Missenden, J., Lecuona, A., & Tozer, R. (2005). A novel experimental investigation of a solar cooling system in Madrid. *International Journal of Refrigeration*, *28*(6), 859–871. doi:10.1016/j.ijrefrig.2005.01.007

The Montreal Protocol on Substances that Deplete the Ozone Layer. (1997). Retrieved October 16, 2014, from http://ozone.unep.org/pdfs/Montreal-Protocol2000.pdf

Kuehn, T. H., Ramsey, J. W., J. L. T. (1998). *Thermal Environmental Engineering*. *Prentice Hall* (3rd ed.). Englewood Cliffs, NJ: Prentice Hall. Retrieved from http://www.amazon.com/Thermal-Environmental-Engineering-3rd-Edition/dp/0139172203

Wilcox, S., & Marion, W. (2008). Users manual for TMY3 data sets, *581-43156*.

Yeung, M. R., Yuen, P. K., Dunn, A., & Cornish, L. S. (1992). Performance of a solar-powered air conditioning system in Hong Kong. *Solar Energy*, *48*(5), 309–319. doi:10.1016/0038-092X(92)90059-J

CURRICULUM VITAE

Mohsen Jahandardoost **Jahandar@unlv.nevada.edu**

Education

University of Nevada, Las Vegas, NV Jan. 2012– Dec. 2014
Master of Science in Mechanical Engineering
Minor: Materials and Mechanics
GPA: 3.82

University of Nevada, Las Vegas, NV Jan. 2013– May. 2014
Graduate Certificate in Solar and Renewable Energy
School of Environmental and Public Affairs

University of Gilan, Rasht, Iran Sept. 2001– Jan. 2006
Bachelor of Science in Mechanical Engineering
Minor: Solid Mechanics

Professional work

Graduate Assistant Aug. 2012–Dec. 2013
University of Nevada, Las Vegas, NV

- Research study on solar thermal absorption cooling system
- Experimental study of different solar collectors
- HVAC leader and LEED analyzer at UNLV's solar decathlon team
- Research study on designing PV and solar hot water system (SAM modeling)
- Teaching EGG 101 Lab., Introductory Engineering Experience

Senior Mechanical Engineer Sept. 2008–Dec. 2011
Jahan Farzan Novin Co., Semnan, Iran

- Coordinated production of 2.5 MW wind turbine blades
- Coordinated installation of composite water tanks (20 – 800 m^2)
- Designed the composite insulation cab for power plant generator
- Designed the composite manhole with SMC composite (EN 124-D 400)
- Designed the composite low voltage power distribution box

Mechanical Engineer Jul. 2005– Sept. 2008
Parmida Refractory Co., Tehran, Iran

- Designed, analyzed, and established characteristic of Heating, Ventilation, and Air Conditioning mechanisms (HVAC)

- Provided technical machine's equipment support
- Reviewed the design of equipment and established maintenance guidelines
- Directed mechanical technicians for upper works

Tools Engineer, Internship Jul. 2004– Sept 2004
Bahman Motor Co. (MAZDA), Tehran, Iran

- Reviewed the CAD maps and produced jig and fixtures related to Mitsubishi Outlander
- Developed and maintained of documents related to Mitsubishi Outlander and Mazda 323 focused on jigs and fixtures
- Maintained strong relationship with field service groups to captured feedback on equipment operation and maintenance issues for Mazda 323 jig and fixture.

Other skills

CATIA V5, Solidworks, and Autodesk, ANSYS, Energy 10, SAM, and Matlab.

Publication

48th AIAA/ASME/ASCE/AHS/ASC Structures, Structural Dynamics, and Materials Conference, Honolulu, Hawaii Apr. 2007
Stress Intensity Factors in Un-repaired and Repaired Cracked Aluminum Panels by CFRP Composite Patch-FE Analysis

Certificate

Building Installation Engineer (PE), Iran Jul. 2011
Global Leadership Retreat, UNLV short course Oct. 2012
OSHA 10, Occupational Safety and Health Administration Aug. 2013

Memberships

ASME (American Society of Mechanical Engineering), 2004
AIAA (American Institute of Aeronautics and Astronautics) 2004
ASHRAE (American Society of Heating, Refrigerating and Air-Conditioning Engineers) 2013

Honor and Scholarship

Tau Beta Pi (Engineering Honor Society) 2013
ASHRAE Scholarship (Chapter of Southern Nevada) 2013
UNLV Access Grant Scholarship 2012– 14
ASPE Scholarship (Southern Nevada Chapter) 2013